HALL SENSOR-BASED LOCKING ELECTRIC DIFFERENTIAL SYSTEM FOR BLDC MOTOR DRIVEN ELECTRIC VEHICLE WITH INDEPENDENT WHEEL DRIVES

by

Milad Gougani

B.A.Sc., Simon Fraser University, 2010

A THESIS SUBMITTED IN PARTIAL FULFILMENT OF THE REQUIREMENTS FOR THE DEGREE OF

MASTER OF APPLIED SCIENCE

in

The Faculty of Graduate Studies

(Electrical and Computer Engineering)

THE UNIVERSITY OF BRITISH COLUMBIA

(Vancouver)

April 2012

ABSTRACT

It is generally known that stability of vehicles under certain driving conditions may be improved by forcing the wheels to turn at the same speed and angle regardless of the available traction under individual wheels. For conventional all-terrain vehicles or sport-utility vehicles, this function can be achieved by locking the mechanical differential system. In this thesis, we propose an innovative approach for locking the electrical differential system (EDS) of electric vehicles (EV) with independent brushless DC (BLDC) machine-based wheel drives. The proposed method locks the active wheels of the vehicle as if they were operating on a common "virtual" shaft. The locking algorithm is implemented by processing the Hall sensor signals of the considered motors and driving them with a single set of "averaged" Hall signals, thereby operating the motors at the same speed and angle. A detailed switch-level model of EDS embedded with the proposed Sync-Lock Control (SLC) along with the BLDC propulsion motors has been developed and compared against measurements for the considered BLDC propulsion motors. The proposed technique is shown to achieve better results compared to a conventional speed control loop as the considered motors are locked directly through the corresponding magnetic fields.

An efficient realization of the proposed controller is presented that makes it possible to be potentially programmed inside existing motor controllers or implemented in a stand-alone microcontroller which can be packaged into a dongle circuit. The proposed SLC is implemented digitally using a programmable integrated circuit microcontroller. First, the Hall signals undergo a layer of filtering to mitigate the errors that are common due to Hall sensor misalignment in low-cost BLDC motors. Then, the locking algorithm is implemented by averaging the filtered Hall sensor signals. The SLC prototype is implemented in form of a standalone dongle-circuit that can be easily placed between the original Hall-sensors and the BLDC motor driver. Operation of typical industrial BLDC motors with the proposed controller is shown to outperform conventional controllers and lock both speed and angle of the motors.

PREFACE

I am the main contributor and the primary author of this thesis and the publications from which it is comprised. I have derived most of the equations, developed all computer models, conducted simulations and experiments, and completed the hardware design and implementation of the proposed electric differential system to achieve the results presented in this thesis.

Some material from Chapters 2 and 3 has been published: M. Gougani, M. Chapariha, J. Jatskevich, "Locking electric differential for brushless DC machine-based electric vehicle with independent wheel drives," *In Proc. IEEE Vehicle Power and Propulsion Conference (VPPC), Chicago*, IL, USA, September 6-9, 2011. I developed the proposed vehicle propulsion model in Matlab/Simulink, verified the model, designed an electric differential system for the propulsion model, conducted simulations and experiments, and proposed hardware implementation methods.

A version of Chapters 4 and 5 has also been published: M. Gougani, M. Chapariha, J. Jatskevich, A. Davoudi, "Hall Sensor-Based Locking Electric Differential System for BLDC Motor Driven Electric Vehicles," *In Proc. IEEE International Electric Vehicle Conference (IEVC),* Greenville, SC, USA, March 4-8, 2012. I designed and developed the hardware implementation of the proposed differential system and wrote most of the manuscript.

The manuscripts used in this thesis, were initiated and prepared by me, and then iterated by the co-authors, Mr. Chapariha and Dr. Jatskevich, to improve quality and coherency of the text. Mr. Chapariha has also helped me conduct some of the hardware experiments presented in Chapter 5. The entire research work presented in this thesis has been supervised by Dr. Juri Jatskevich, and he has also helped me throughout the research with his invaluable ideas and guidance. The work presented in my thesis extends some of the previous projects supervised by Dr. Jatskevich in the area of brushless motors.

TABLE OF CONTENTS

Abstract ..... **ii**

Preface ..... **iii**

Table of Contents ..... **iv**

List of Tables ..... **vi**

List of Figures ..... **vii**

Acknowledgements ..... **ix**

1 Introduction **1**

1.1 Electric Vehicle Configuration 2

1.2 Electric Propulsion System with Brushless DC Motors 4

1.3 Electrical Differential System 7

1.4 Objectives and Summary of Contributions 7

2 Detailed Model of Electric Vehicle Propulsion System **9**

2.1 Introduction 9

2.2 Hall Sensor Controlled BLDC Motor-based Drive System 10

2.2.1 Detailed Model of the Electrical System 10

2.2.2 Electrical Model Verification 13

2.3 Vehicle Mechanical Dynamics 15

2.3.1 Detailed Model of the Mechanical Subsystem 15

2.4 Electric Vehicle Propulsion System Model 17

3 Detailed Model and Simulation of Locking Electric Differential System **19**

3.1 Introduction 19

3.2 Synchronization and Locking Techniques 20

3.2.1 Conventional Speed Control 20

3.2.2 Proposed Sync-Lock Control 21

3.3 Simulation Case Studies 27

3.3.1 Sync-Lock Controller Transient 27

3.3.2 Load Step Transient 29

3.3.3 Emulated Driving Condition 31

4 Implementation for Low Precision Brushless DC Motors **32**

4.1 Introduction 32
4.2 Brushless DC Motors with Unbalanced Hall-Sensors 33
4.2.1 Filtering Hall-Sensor Signals 33
4.3 Implementation of SLC with Correction for Hall Sensor Misalignment 35
4.3.1 Digital Implementation of Hall-Sensor Signals Filtering 35
4.3.2 Implementation of Hall-Sensor Signals Locking 38
4.3.3 Combined Implementation of Filtering and Locking of Hall-Sensor Signals 39
5 Hardware Realization Using PIC Microcontroller 41
5.1 Introduction 41
5.2 Algorithm Implementation and Hardware Prototype 42
5.2.1 Digital Implementation of EDS 42
5.2.2 Hardware Prototype 45
5.3 Experimental Case Studies 47
5.3.1 Sync-Lock Controller enabling Transient 47
5.3.2 Transient due to Change in Load 48
6 Conclusions and Future Work 50
6.1 Conclusion 50
6.2 Future Work 51
Bibliography 52
Appendices 55
Appendix A: Parameters used for Studies in Chapters 2 and 3 55
Appendix B: Parameters used for Studies in Chapter 4 and 5 56
Appendix C: Designed PCB Schematic 57
Appendix D: Designed PCB Layout (Double Sided) 58

LIST OF TABLES

Table 2.1 Sample Adhesion Coefficient Parameters 16

Table 3.1 Hall sensor states as a function of rotor position 22

Table 3.2 Standard switching intervals of a 120-degree inverter 23

LIST OF FIGURES

Figure 1.1 Conceptual electric vehicle configuration. 3

Figure 1.2 Considered electric vehicle propulsion system configurations: (a) independent drive wheels with motor-gear assembly outside the wheels; (b) independent drive wheels with motors outside coupled through fixed gearing inside the wheels; and (c) independent drive wheels with traction motors connected directly to the wheels with no gearing..... 4

Figure 1.3 BLDC motor-drive system: (a) schematic configuration BLDC motor-drive system; and (b) Hall sensor configuration of the prototype BLDC motor. 6

Figure 2.1 Electric vehicle propulsion sub-system. 9

Figure 2.2 BLDC motor-drive system. 10

Figure 2.3 Three phase BLDC machine with Hall sensors. 11

Figure 2.4 Hall sensor signals of a BLDC motor. 13

Figure 2.5 Electric model verification: (a) experimental setup of BLDC propulsion motor prototype under test; and (b) measured and simulated phase currents and voltages. 14

Figure 2.6 Example of Adhesion coefficient functions for dry and wet conditions. 16

Figure 2.7 Mechanical forces acting on one wheel. 16

Figure 2.8 Block diagram of the electric vehicle propulsion system model composed of the electrical model of the BLDC motor-drive system and mechanical dynamics of the vehicle and wheels. 18

Figure 3.1 BLDC motor-drive system with the proposed Sync-Lock Controller. 20

Figure 3.2 Conventional EDS speed control using PI loops. 21

Figure 3.3 EDS speed control with the proposed SLC. 21

Figure 3.4 Proposed averaging of the Hall sensor signals for the SLC. 22

Figure 3.5 Analog implementation of the SLC that enables the timing of the input and output Hall signal transitions. 24

Figure 3.6 Timing of the input and output Hall signal transitions using the analog implementation of the proposed SLC. 25

Figure 3.7 Timing of the input and output Hall signal transitions using the proposed digital implementation of the SLC. 26

Figure 3.8 Simulated transient of the vehicular system when the proposed SLC is activated. 28

Figure 3.9 Speed and electromagnetic torque transient response due to load change when the EDS uses with conventional control. 29

Figure 3.10 Speed and electromagnetic torque transient response due to load change when the EDS uses proposed SLC. 30

Figure 3.11 Difference in motor shafts angles using conventional and proposed synchronization approaches. 30

Figure 3.12 System response to emulated bumpy road when EDS uses conventional and proposed SLC control. 31

Figure 4.1 Proposed two-BLDC motor-drive vehicular propulsion system. 32

Figure 4.2 Stator currents with unequal conduction intervals due to Hall-sensor misalignment [24]. 33

Figure 4.3 Timing of the input and output Hall signal transitions. 37

Figure 4.4 Timing of the input and output Hall signal transitions (averaging). 38

Figure 4.5 Timing of rising edge input and output interrupts. 39

Figure 4.6 Timing of falling edge input and output interrupts. 40

Figure 5.1 Experimental system setup. 41

Figure 5.2 Flow chart of conditions and functions performed during input the ISR. 43

Figure 5.3 Flow chart of the software output ISR. 45

Figure 5.4 Input and output Hall signal transitions using the proposed averaging. 45

Figure 5.5 Prototype dongle-filter for use with existing motor drivers: (a) actual-size photo of the printed circuit board; and (b) simplified block-scheme representation depicting major components and ports. 46

Figure 5.6 Measured phase current and speed transient response of both motors due to enabling the proposed SLC. 47

Figure 5.7 Measured mechanical torque and speed transient response due to load change with proposed SLC disabled. 48

Figure 5.8 Measured mechanical torque and speed transient response due to load step up with proposed SLC enabled. 49

Figure 5.9 Measured mechanical torque and speed transient response due to load step down with proposed SLC enabled. 49

ACKNOWLEDGEMENTS

I would like to acknowledge and extend my heartfelt gratitude to faculty, staff and my fellow colleagues at the UBC Electrical Energy and Power Systems lab. I owe particular thanks to Dr. Juri Jatskevich, whose invaluable guidance and continuous support enabled me to complete this thesis. It has been an honor for me to work with such a committed and knowledgeable individual. I would like to acknowledge the financial support from the Natural Science and Engineering Research (NSERC) Discovery Grant lead by Dr. Jatskevich as well as from Institute for Computing, Information and Cognitive Systems (ICICS) that enabled my traveling and presentation of our publications on prestigious IEEE conferences. I also thank Dr. Dommel and Dr. Dunford, who have kindly accepted to be on my examining committee and devote their time and expertise, for their constructive comments, feedback and advice.

I would also like to thank my colleague, Mr. Mehrdad Chapariha, for his help and constructive suggestions during our collaboration. My warm appreciation goes to all members of the UBC Electrical Energy and Power Systems Group who have supported me throughout my program at UBC.

Special thanks are owed to my family and my friends. My words alone cannot express what I owe to them for their encouragement and support throughout my years of education, both morally and financially.

1 INTRODUCTION

In recent years, there has been a significant emphasize on research and development of high-efficiency, clean, and safe alternative to internal combustion (IC) engine vehicles. This surge to replace IC vehicles was fueled by environmental and economical problems caused by large number of automobiles used around the world and the problems that they create. Problems such as air pollution, global warming, and the rapid depletion of petroleum resources are now of paramount concern. Electric vehicles (EV) have been typically proposed as the solution to a clean transportation. Electric vehicles have been around for centuries but have not yet been able to compete with internal the more conventional IC vehicles that have much higher ranges and are very easy to refuel.

The first EV was built by Frenchman Gustave Trouvé in 1881. It was a tricycle powered by a 0.1 hp DC motor fed by lead-acid batteries [1]. But the EV did not attract much attention from the public until the 1864 Paris to Rouen race: the 1135 km were run in 48 hr and 53 min at an average speed of 23.3 km/h. The following few years marked the era of EVs. The first commercial EV was the Morris and Salom's Electroboat. These vehicles used as taxis in New York City could operate for three shifts of 4 hr with 90-min recharging periods in between. They were powered by two 1.5 hp motors that allowed a maximum speed of 32 km/h and a 40 km range [1]. In 1897, Frenchman M. A. Darracq introduced the concept of regenerative braking which is considered as one of the most significant contributions to the EV technology. Another significant contribution of the era was the "La Jamais Contente", first EV ever to reach 100 km/hr, built by yet another Frenchman Camille Jenatzy. But as the gasoline cars became more powerful and easier to operate, EVs started to disappear. The invention of transistor in 1945 was expected to help revive EVs as it made it possible to regulate the power fed to an electric motor without the very inefficient rheostats and allowed the running of AC motors at variable frequency [2]. But the expectations were only realized in space with the Lunar Roving Vehicle used on the moon by Apollo astronauts. Although there has been few attempts since then to bring back EVs, it was only in late 2000^{th} that EVs became "mainstream" again with the introduction of Tesla Roadster, Chevy Volt, Nissan Leaf and Fisker Karma just to name a few. Today, with new developments in energy storage and management systems (such as advances in battery and fuel cell technology) coupled with environmental concerns and depreciation of petroleum resources, there is a high probability of ICs being replaced by EVs.

In this thesis we will design and develop a differential system (DS) for an EV with a modern configuration. In a typical vehicle configuration, e.g., such as a sport utility or an all-terrain vehicle, a differential system is used to couple the driving wheels and at the same time allow the wheels to rotate at different speeds. This is necessary for a smooth ride and soft cornering when one wheel (outside of the

turning curve) rolls farther and faster than the other one (inside of the turning curve). Another very important function of the differential system is the traction control. The idea is to maximize usable traction of the vehicle with the differential system. The low traction situation occurs when one wheel spins faster than the other one under certain road conditions. To maximize the vehicle traction, the differential system can lock both wheels and forcing them to turn at the same speed and angle regardless of which wheel has more traction.

This thesis focuses on a modern EV configuration with independent drive wheels and reduced mechanical components. With the considered EV configuration and independent drive wheels, the locking of differential system is not just necessary in the absence of mechanical shaft also becomes an essential component for providing the driver with increased safety and confidence when traveling on wet or icy roads, gravel, mud and dirt. The electronically controlled actuation provides rapid response for stability and traction control. The objective of thesis is to develop a locking electric differential system (EDS) for independent wheel driven EV. In this thesis, an innovative locking EDS has been proposed, developed and tested on a two wheel drive system. However, proposed locking methodology is very general and can be readily extended to any number of driving wheels.

1.1 Electric Vehicle Configuration

Automobiles, as one of the greatest achievements of modern technology, are in the verge of complete technological transformation. Internal combustion (IC) engines are being phased out due to their heavy environmental impact and unsustainable operation. Electric vehicles (EVs), hybrid electric vehicles (HEVs), and fuel cell vehicles have been typically proposed to replace conventional vehicles in the near future. In the process of this technological development, the traditional IC vehicle configurations are also being reconsidered as they are no longer suitable for optimum operation of electric counterparts. A concept of a modern electric vehicle configuration considered in this thesis is illustrated in Figure 1.1.

In the basic EV configuration considered herein, drive train consists of three main subsystems: electric propulsion, energy source, and auxiliary systems [2]. Electric propulsion subsystem, which is focus of this thesis, is comprised of a vehicle controller, power electronic converters, and electric motors (driving wheels). Control inputs from the accelerator and brake pedal along with steering are fed to the vehicle controller. Controller in turn operates the power electronic drive which regulates power flow between the electric motor and energy source. The energy source subsystem includes energy storage, energy management unit, and a charger. Finally, auxiliary subsystem manages power steering units and the interior auxiliary devices.

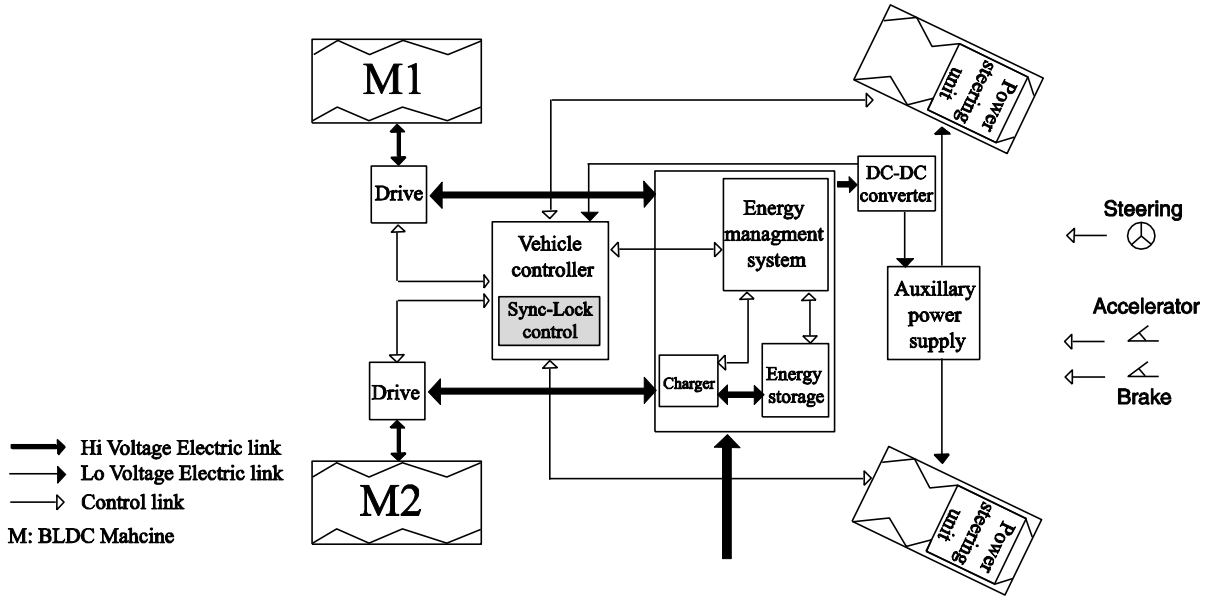

Figure 1.1 Conceptual electric vehicle configuration.

To simplify the mechanical part of EV, independent wheel configuration is often considered, where the mechanical differential is replaced by using separate (independent) traction motors. Traction motors can either be placed inside the wheel or linked to the wheel through a mechanical gearing. In either configuration, there is no common mechanical shaft connecting any of the wheels together. Instead, an electric differential system (EDS) is used to distribute the mechanical (traction) load among the propulsion motors, as well as implement any special functions such as synchronization and/or locking of the motors relative to each other.

In general, there may be many possible propulsion system configurations with independent wheels. Without loss of generality, in most of this thesis we consider a propulsion system with two driving (and two driven) wheels. Some commonly used configurations of the vehicle driving wheels are shown in Figure 1.2. Figure 1.2 (a) shows the configuration of an independent-wheel with traction motor being outside and linked through some fixed gearing. Drive train can be simplified by placing motor-gear assembly inside the wheel as shown in Figure 1.2 (b). A thin planetary gear may be used in this configuration to reduce the motor speed and enhance propulsion torque. The gear arrangement not only offers high-speed reduction ratio but also provides an inline arrangement of input and output shaft. In Figure 1.2 (c), the mechanical gear is abandoned and rotor of the electric motor is directly connected to driving wheel. In this arrangement, controlling speed of the electric motor is equivalent to controlling the wheel and hence the vehicle speed. The electric propulsion system model developed in this thesis is very general and can be readily extended to any one configuration depicted in Figure 1.2.

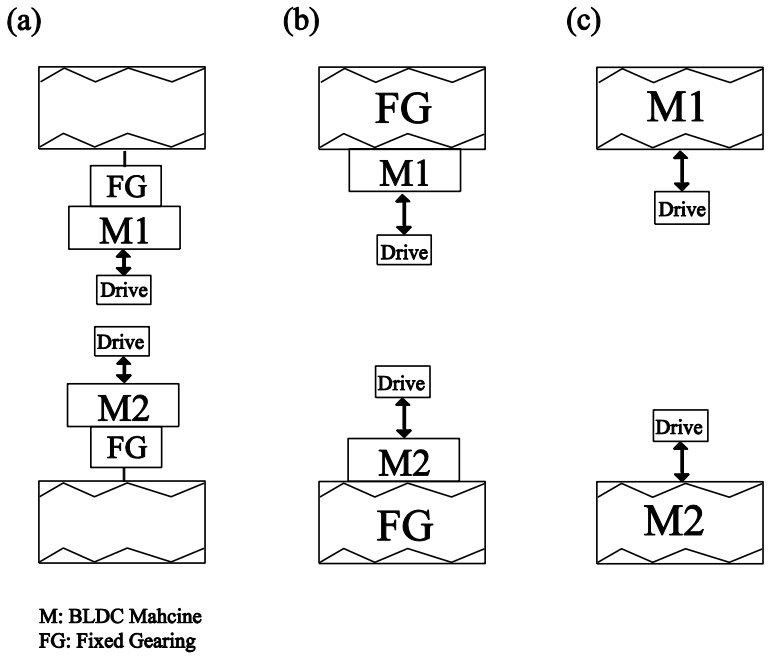

Figure 1.2 Considered electric vehicle propulsion system configurations: (a) independent drive wheels with motor-gear assembly outside the wheels; (b) independent drive wheels with motors outside coupled through fixed gearing inside the wheels; and (c) independent drive wheels with traction motors connected directly to the wheels with no gearing.

1.2 Electric Propulsion System with Brushless DC Motors

An electric propulsion system is the heart of an electric vehicle. Choice of an electric motor for the propulsion system depends on a number of factors. This section provides a brief overview of motor drives suitable for EVs including brushless DC motors. Conventional brushed dc motors have been used for centuries in urban transit systems or locomotive drives. However, dc motors require frequent maintenance and are expensive to operate. Induction motors require much less maintenance. Although induction motors are rugged, the complexity of inverter control circuits, the relatively lower efficiency and the power factor associated with these motors, have not made them preferred in some applications. Considering the fact that synchronous motors have fewer maintenance problems than dc motors and have higher efficiency than induction motors, it is only logical to consider them as a viable and reliable solution for electric vehicle propulsion. Synchronous motors with solid state control have been investigated quite well for years and have proven to be a viable option for applications with variable-speed drive systems such as electric vehicles. In many high-power industrial applications (mills, grainer, etc.) synchronous motor drive system are based on self-controlled thyristors that are very simple, cost effective, and reliable.

A permanent magnet synchronous motor (PMSM), also known as brushless DC (BLDC) motor, is considered here for the electric vehicle propulsion system. BLDC motor is as rugged as an induction motor and has great potential for applications with variable speed drive systems. Furthermore, the solid state power conditioners for BLDC motors are simpler and less expensive than those required for induction motors. It should also be mentioned that BLDC motor drive systems require rotor position sensors, power electronics (inverters), and complex controllers. A typical BLDC motor consists of a permanent magnet synchronous machine (PMSM) fed with a voltage source inverter (VSI). As rotor magnets typically have high electrical resistance, rotor losses are small, resulting in higher efficiency. VSI is powered by a dc source. And switching logic of inverter is always determined with respect to the rotor position, which ensures synchronous operation at variable frequency. Approaches to establish rotor position are generally classified into two categories; sensorless and sensor-based. Although there has been many publications on sensorless position estimation schemes [3]–[6], sensor based drives are still preferred due to their simple implementation and reliable operation under different loading conditions and speeds, without the need for machine parameters. Figure 1.3 (a) below illustrates general layout of a Hall-sensor controlled BLDC motor-drive system. Sensorless techniques are typically based on using measured voltages and/or currents [7]–[9], the back emf generated in stator windings [10]–[11], or the observer-based methods [12]–[13]. Furthermore, sensorless approach is not very reliable in low speeds and generally requires significant computational resources to operate the motor. A brief summary of BLDC motor advantages properties can be found in [3], and includes the following:

- Small rotor size and high power density
- Low inertia and faster dynamic response
- High speed and torque capability
- Low or no maintenance
- High torque/inertia ratio
- Good heat dissipation due to the stationary armature winding. More cross-sectional area for armature windings which improves conduction of heat through the frame.

For low-cost BLDC motor drive systems such as those suitable for automotive applications, Hall-sensor-based approach is probably the most common for estimating rotor position as it avoids expensive position encoders on the motor or the vehicular wheels. This method is simple, economical, and very reliable. As shown in Figure 1.3 (b), in this configuration, three Hall sensors are positioned 120 degrees apart and react to a magnetic tablet that mimics magnetic characteristics (poles) of the rotor. Each Hall sensor outputs a digital signal dictated by their interaction with the rotor magnetic poles. With this arrangement, one mechanical revolution is divided into six different zones. Combined state of the three Hall-sensor signals is used to identify the zone in which rotor is located. Inverter transistors are then

switched accordingly to produce the desired electromagnetic torque. Unlike sensorless approaches, the Hall-sensor-based BLDC drive systems are self-starting, very reliable, and have good and predictable torque-speed characteristic in wide range of speeds. Hall-sensor-based drive system require much less computational resources as it is based on a look-up table that maps each of the six states of the Hall-sensor signals to the corresponding topology state of the VSI. Another advantage of this drive system is its high compatibility. Most of the industrial BLDC drives simply accept Hall sensor signals as an input without any specific requirements.

The back emf in a typical BLDC motor may be either trapezoidal or sinusoidal [14], [16] depending on the rotor construction. As the sinusoidal back emf is generally harder to achieve, motors with trapezoidal back emf tend to be less expensive and widely available. The thyristors may be controlled using the 180- or 120-degree commutation logic [14], [3]. 180-degree switching logic is better suited for PWM-generating of sinusoidal stator currents in motors with sinusoidal back emf. In this method, each phase is always connected either to positive or negative bus of the inverter. 120-degree switching is used extensively with trapezoidal back emf machines. In this method, each stator phase is conducting for 120 electrical degrees and is then left floating for 60 electrical degrees, which happens two times during one electrical revolution. This thesis is primarily focused on Hall-sensor-controlled trapezoidal BLDC motors that are more widely used because of their simplicity and robustness.

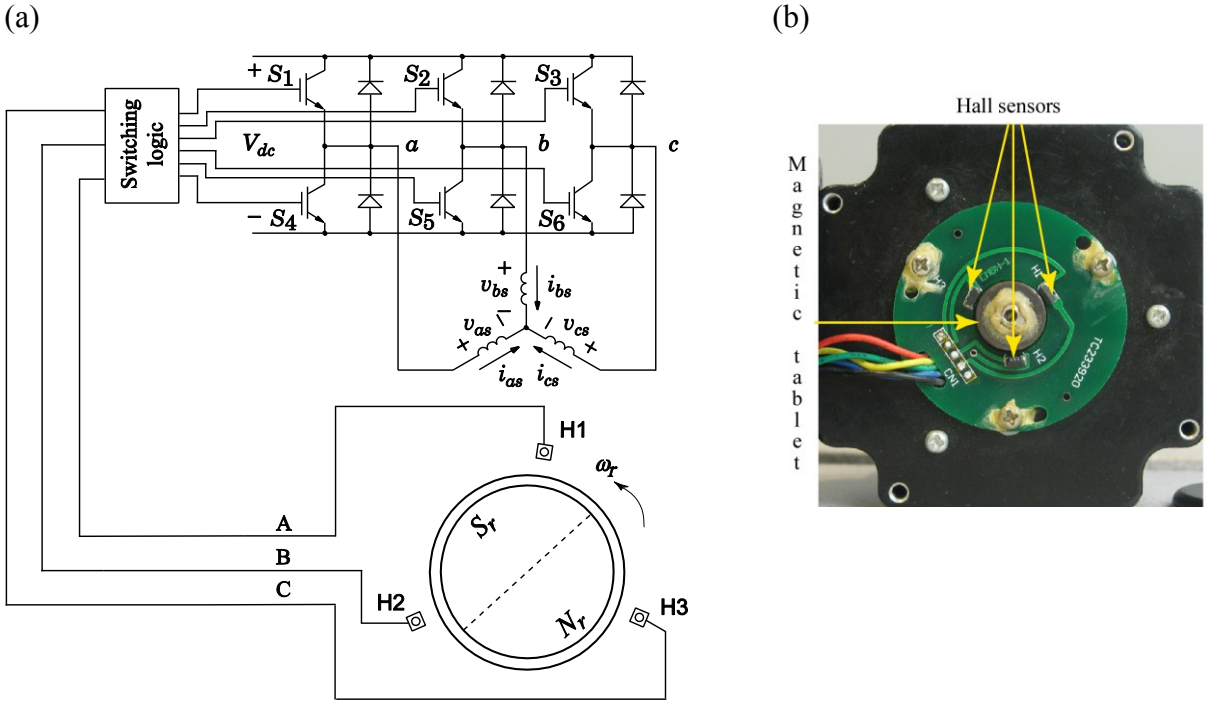

Figure 1.3 BLDC motor-drive system: (a) schematic configuration BLDC motor-drive system; and (b) Hall sensor configuration of the prototype BLDC motor.

1.3 Electrical Differential System

In general, stability of vehicles under certain driving conditions can be improved by forcing the wheels to turn at the same speed regardless of the available traction under individual wheels. For conventional vehicles this can be achieved by forcing the wheels to run on a common shaft which is done through locking the mechanical differential system. This cannot be done on the proposed platform of Figure 1.1 as there is no mechanical link between the two wheels. Hence, the operation of the mechanical differential system needs to be emulated electronically for the independent-wheel drive train through what is known as an electric differential system (EDS). In this thesis, we propose an innovative approach for locking electrical differential system of EVs with independent BLDC machine-based wheel drives [17]-[18].

1.4 Objectives and Summary of Contributions

This thesis is focused on an electric propulsion system of an electric vehicle with independent-wheel drive train as shown in Figure 1.1. The propulsion system considered in the thesis is based on Hall-sensor controlled BLDC motor-drive subsystem. The specific objective of the thesis is to propose a simple and effective Sync-Lock Control (SLC) method for considered propulsion system. The controller is used to lock the wheels (i.e. motors) by forcing them to turn at the same speed regardless of the available traction under individual wheels which helps to improve stability of the vehicle under certain driving conditions [17], [18]. The controller is developed with reliability issues and economic aspects in mind. Proposed solution is also expected not to compromise robustness of the Hall-sensor-based drive systems and not to impose addition of expensive components to conventional drives.

In this thesis, the proposed controller is implemented using an innovative algorithm that is based on merging Hall sensor signals of two BLDC motors and running both motors with a single set of combined signals. The developed algorithm is fundamentally different from conventional methods, such as speed or position PI controllers, etc., in that both speed and position of the motors become locked internally through corresponding magnetic fields of the participating machines. The proposed locking technique is novel. To the best of our knowledge, Hall signals have not been considered in the past for locking/synchronizing multiple BLDC motors.

An analog and a digital realization of the proposed algorithm are tested in MATLAB Simulink [22] on a detailed model of an electric vehicle propulsion system. The overall model is composed of BLDC motor-drive systems integrated with mechanical subsystem of the vehicle, which includes vehicle body and the wheels. In addition to the analytical and modeling work, a hardware prototype of the developed algorithm has been realized on a 16-bit Digital Signal Processing Microcontroller (dsPIC30F2020) in

form of a standalone dongle-circuit. The fabricated circuit has been tested and verified experimentally on a number of typical industrial BLDC motors and drivers. Additionally, a correction filter proposed in [19], [20], and [21] has been integrated into the proposed controller in order to accommodate practical low-cost BLDC motors with misaligned Hall sensors. The summary of the overall contributions presented in this thesis include the following:

- A simple and yet effective control-level averaging approach is proposed to synchronize (lock) the operation of the driving motors and equalize their speed and position.
- Straightforward and computationally efficient analog and digital implementations of the proposed Sync-Lock Control are presented and verified in MATLAB/Simulink.
- The proposed Sync-Lock Controller is realized in hardware in the form of a standalone dongle-circuit that can be placed between the original Hall-sensors and the motor drive to process the signals and filter out all undesirable errors in the signals. A compact prototype of the proposed dongle had been fabricated and tested on a number of typical industrial BLDC motors and drivers.
- The thesis presents extensive simulations as well as the experimental results with the hardware prototypes to validate the effectiveness of the proposed generalized methodology.

2 DETAILED MODEL OF ELECTRIC VEHICLE PROPULSION SYSTEM

2.1 Introduction

The conceptual drive train configuration of the electric vehicle was introduced in Chapter 1. The considered drive train consists of three main subsystems: electric propulsion, energy source, and auxiliary systems [2]. The electric propulsion subsystem, which is focus of this thesis, is comprised of a vehicle controller, power electronic converters, and two electric motors (driving wheels) as shown in Figure 2.1. Without loss of generality, the two BLDC propulsion motors are assumed for vehicle propulsion system, whereas the model can easily be extended for any number of driving wheels. Control inputs from the accelerator and brake pedal along with steering are fed to the vehicle controller. Controller in turn operates the power electronic drive which regulates power flow between the electric motor and the energy source. Since in electrical vehicles similar to that depicted in Figure 2.1 there is no common mechanical shaft or transmission that can be used for locking the wheels, this function has to be achieved by means of electronic control that enables locking of the electrical differential system (EDS) [17].

Without loss of generality, electric propulsion system of the vehicle is based on a pair of BLDC motors with Hall-sensor-based controls. In this Chapter, first a detailed model of the BLDC motor-drive system is developed and implemented in MATLAB Simulink [22] using the toolbox [23]. The model is then verified by carrying out experiments using several commercially available BLDC Hall-sensor-based drivers as well as a prototype driver [24]. Furthermore, a model of a mechanical subsystem of EV is developed to be integrated with electrical model of the drive system. Mechanical subsystem is composed of the vehicle body and the wheels system. Having established the models of both electrical and mechanical subsystems, different methodologies for locking and synchronizing the independent wheels (motors) are objectively evaluated in the next chapter.

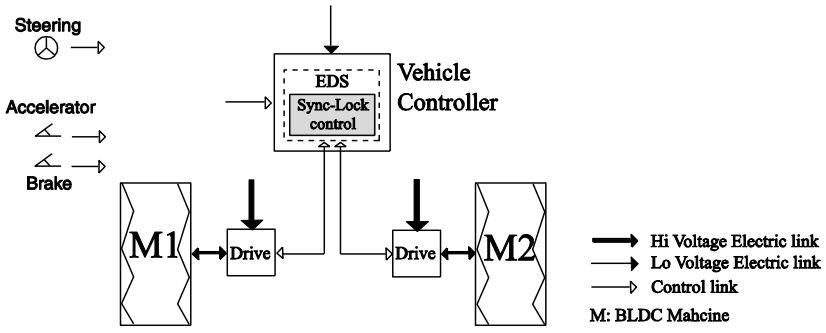

Figure 2.1 Electric vehicle propulsion sub-system.

2.2 Hall Sensor Controlled BLDC Motor-based Drive System

A BLDC motor consists of a permanent magnet synchronous machine (PMSM) supplied with an inverter. In this type of motor switching of the inverter is determined by rotor position. Generally, the approaches to establish rotor position may be classified into sensor and sensorless methods [25], [9], and [3]. The method that uses Hall Effect sensors has numerous advantages, especially at low speeds where many sensorless methods become less practical. In this thesis, we focus on Hall-sensor-driven BLDC motors since these are the most cost effective and mass-produced. Details of a BLDC motor-drive system schematic are shown in Figure 2.2. Here, the Hall sensors H1, H2 and H3 provide inverter with rotor position information which is necessary to control inverter transistors according to the standard 120-degree switching logic [27].

2.2.1 Detailed Model of the Electrical System

The BLDC machines are often considered in various electromechanical applications, and in general have been investigated quite well in the literature [3] and [26]–[28]. A detailed model of a BLDC machine shown in Figure 2.3 is considered to be incorporated into the electric vehicle model. Based on the commonly used assumptions, the stator voltage equation may be expressed as:

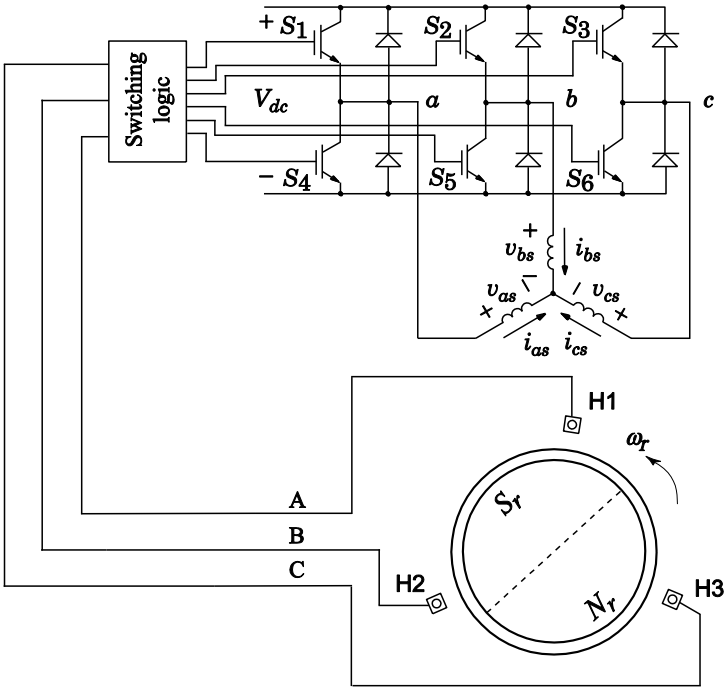

Figure 2.2 BLDC motor-drive system.

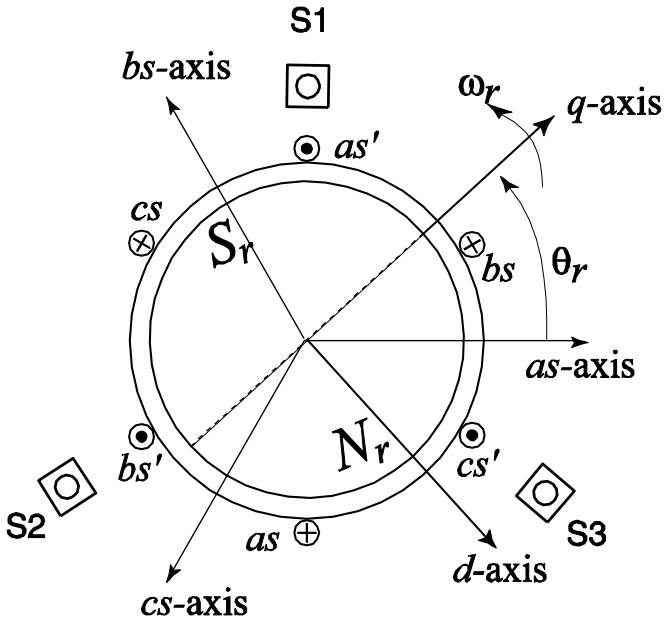

Figure 2.3 Three phase BLDC machine with Hall sensors.

$$\mathbf{v}_{abcs} = \mathbf{r}_s \mathbf{i}_{abcs} + \frac{d\boldsymbol{\lambda}_{abcs}}{dt}, \tag{2-1}$$

Here, the phase variables are arranged in vectors as $\mathbf{f}_{abcs} = \begin{bmatrix} f_{as} & f_{bs} & f_{cs} \end{bmatrix}^T$, where f may represent the voltage, current or flux linkage vectors; and $\mathbf{r}_s$ represents the stator resistance matrix. In the case of a motor with non-sinusoidal back emf, the back emf is assumed to be half-wave symmetric and contains spatial harmonics. Therefore, the stator flux linkages and electromagnetic torque may be written as [28]:

$$\boldsymbol{\lambda}_{abcs} = L_s \mathbf{i}_{abcs} + \lambda'_m \sum_{n=1}^{\infty} K_{2n-1} \begin{bmatrix} \sin\left((2n-1)\theta_r\right) \\ \sin\left((2n-1)\left(\theta_r - \frac{2\pi}{3}\right)\right) \\ \sin\left((2n-1)\left(\theta_r + \frac{2\pi}{3}\right)\right) \end{bmatrix}, \tag{2-2}$$

$$T_e = \frac{3P}{4}\lambda'_m \sum_{n=1}^{\infty} K_{2n-1} \begin{bmatrix} i_{as} \\ i_{bs} \\ i_{cs} \end{bmatrix}^T \cdot \begin{bmatrix} \cos((2n-1)\theta_r) \\ \cos\left((2n-1)\left(\theta_r - \frac{2\pi}{3}\right)\right) \\ \cos\left((2n-1)\left(\theta_r + \frac{2\pi}{3}\right)\right) \end{bmatrix}, \quad (2\text{-}3)$$

where the equivalent stator inductance $L_s = L_{ls} + 1.5L_m$, and the inductance matrix given by

$$\mathbf{L}_s = \begin{bmatrix} L_{ls}+L_m & -0.5L_m & -0.5L_m \\ -0.5L_m & L_{ls}+L_m & -0.5L_m \\ -0.5L_m & -0.5L_m & L_{ls}+L_m \end{bmatrix}, \quad (2\text{-}4)$$

with L_{ls} defined as the stator leakage inductance and L_m as the stator magnetizing inductance. In (2-2) and (2-3), λ'_m is the magnitude of the fundamental component of the permanent magnet (PM) rotor flux linkage. Finally, the coefficients K_n represent the magnitude of the n^{th} harmonic of the flux relative to fundamental component normalized such that $K_1 = 1$.

Detailed model of the BLDC motor is run with an inverter as shown in Figure 2.2. The inverter itself is controlled using standard 120 degree, 6 step inverter commutation scheme. Given the standard 120 degree switching logic, Hall sensors signals will be displaced by 120 electrical degrees as shown in Figure 2.4. This means that every 60 electrical degrees of rotation, one of the Hall sensors changes its state. Therefore, it takes six steps to complete one electrical cycle which is $(P/2)$ times mechanical cycle where P denoted the number of magnetic poles. Figure 2.4 also shows the combined signal which is produced by adding all three Hall sensor signals. Inverter transistors are switched every time the combined Hall signal changes its state, which ideally should be every 60 electrical degrees.

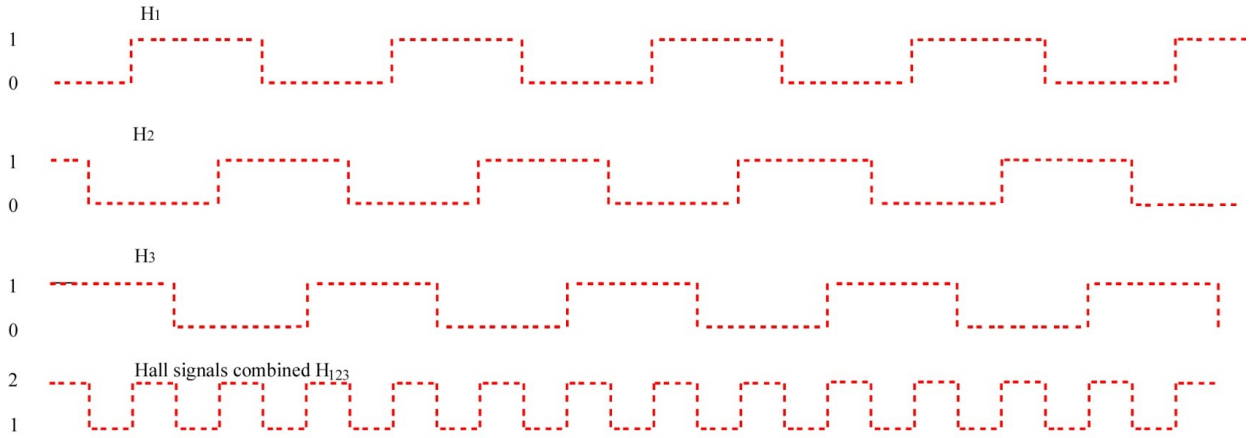

Figure 2.4 Hall sensor signals of a BLDC motor.

2.2.2 Electrical Model Verification

For the EV described in this thesis, prototype BLDC motors whose parameters are summarized in Appendix A are considered. Detailed model of the system was developed and implemented in MATLAB Simulink [22] using toolbox [23]. The 120-degree inverter logic was implemented according to standard table [27], [25], [9]. The model is verified by carrying out experiments using several commercially available BLDC Hall-sensor-based drivers as well as a prototype driver [24] as shown in Figure 2.5 (a), all producing the same results. For this study, an operating point defined by a 330W mechanical load is considered. The motor inverter was supplied with $V_{dc} = 26V$, resulting in a speed of 2140 rpm under the given mechanical load. Measured phase currents and voltages were captured and are shown in Figure 2.5 (b). Simulated phase currents and voltages for the same steady state operating condition are also shown in Figure 2.5 (b). As can be seen, detailed model predicts phase currents and voltages very closely and agrees with measured waveforms. This study confirms accuracy of the developed detailed model, which is used in further studies.

(a)

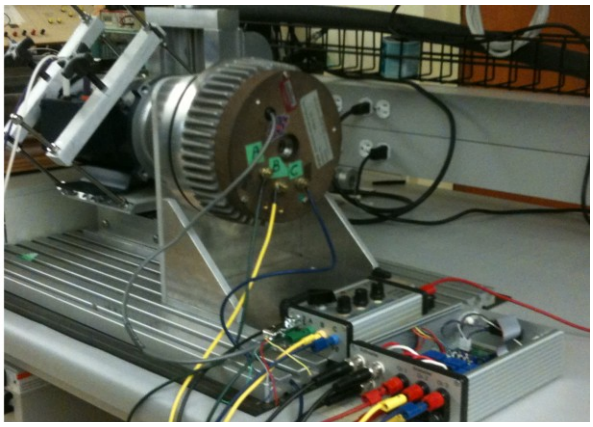

(b)

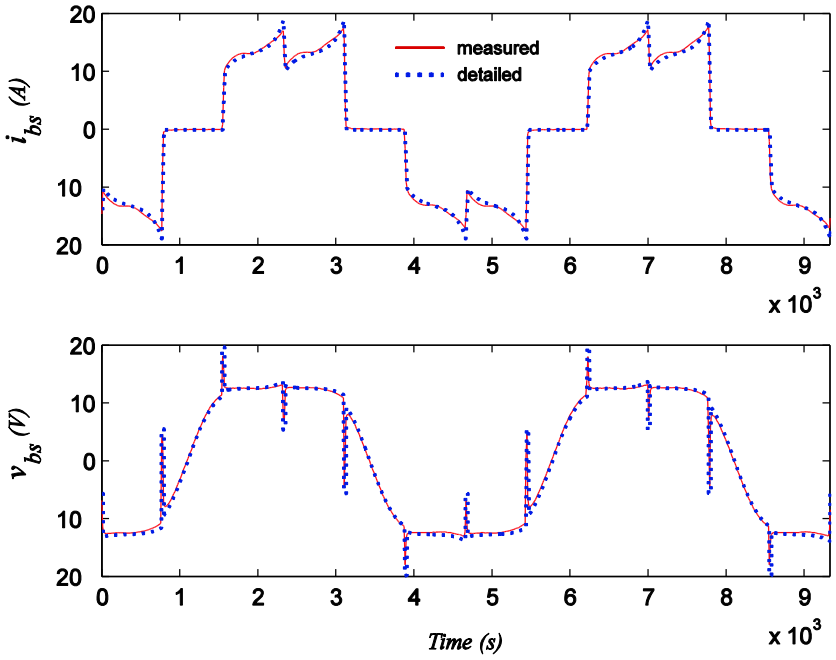

Figure 2.5 Electric model verification: (a) experimental setup of BLDC propulsion motor prototype under test; and (b) measured and simulated phase currents and voltages.

2.3 Vehicle Mechanical Dynamics

2.3.1 Detailed Model of the Mechanical Subsystem

Mechanical subsystem consists of the vehicle body and the wheels system. Dynamics of the vehicle body motion, under the assumption of running on a flat surface, is assumed to have the following form

$$M\frac{dv}{dt} = F_m - R(v), \tag{2-5}$$

where M is the total vehicle and wheel mass, F_m is the drive force, g is the gravitational constant, v is the vehicle velocity and $R(v)$ reflects the running resistance. Opposing resistive force, $R(v)$, is defined empirically in [29] and is assumed to be represented by the following expression

$$R(v) = 1.867 + 0.0359v + 0.000745v^2 \tag{2-6}$$

Dynamics of each drive-wheel-system may be expressed as

$$T_e = J\frac{d\omega_{rm}}{dt} + B_m\omega_{rm} + T_m, \tag{2-7}$$

where ω_{rm} is the rotor mechanical speed, J is the combined inertia of wheel and rotor, and B_m is the damping coefficient associated with mechanical rotational system of the machine. Given r as wheel radius, mechanical load torque on each motor is

$$T_m = f_m r, \tag{2-8}$$

with the drive force defined by

$$\begin{aligned} f_m &= \mu(v_{slip})N \\ &= \mu(v_{slip})mg, \end{aligned} \tag{2-9}$$

where m is the mass subjected to each drive-wheel-system and μ is the adhesion coefficient described by nonlinear function of slip velocity as follows [30]

$$\mu(v_{slip}) = a\cdot e^{-b\cdot v_{slip}} - c\cdot e^{-d\cdot v_{slip}}. \tag{2-10}$$

Here, slip velocity is defined as the difference between wheel and vehicle speed. It may be expressed as follows

$$v_{slip} = v_{wh} - v = r\omega_{rm} - v. \tag{2-11}$$

Table 2.1 Sample Adhesion Coefficient Parameters

	a	*b*	*c*	*d*
μ_0 **(dry)**	1	0.54	1	1.2
μ_1 **(wet 1)**	0.2	0.54	0.2	1.2
μ_2 **(wet 2)**	0.08	0.05	0.08	0.5

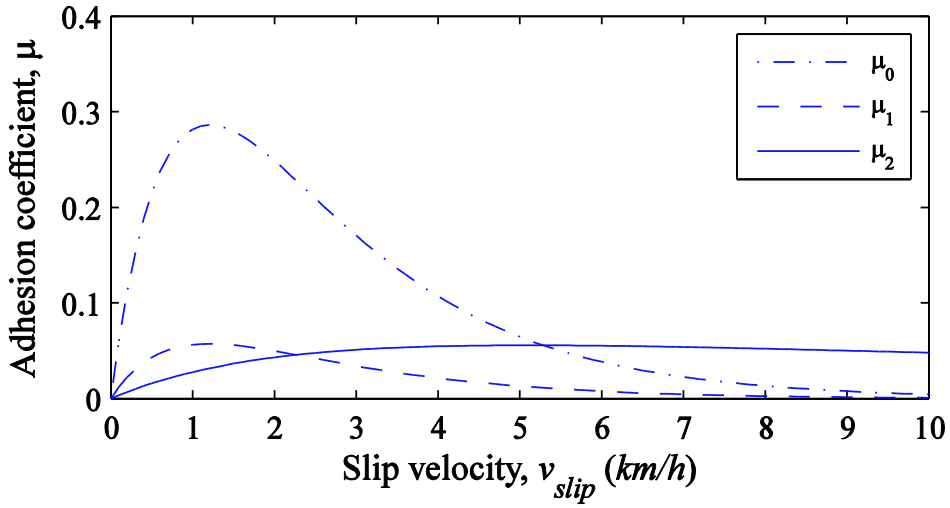

Figure 2.6 Example of Adhesion coefficient functions for dry and wet conditions.

Adhesion coefficients corresponding to the parameters in Table 2.1 are illustrated in Figure 2.6 as a function of slip velocity. The parameters a, b, c, and d are defined based on road surface conditions. Table 2.1 summarizes parameters for three different conditions. The mechanical subsystem dynamics given by (2-5) and (2-7) are summarized below in Figure 2.7.

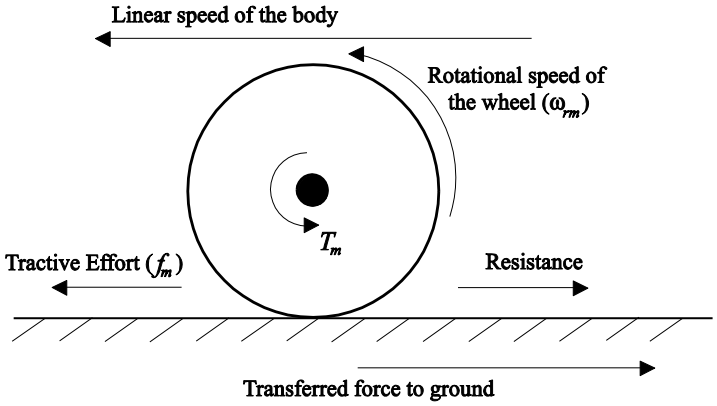

Figure 2.7 Mechanical forces acting on one wheel.

Next mechanical dynamics are integrated into the model by loading the motors according to (2-8) – (2-11). In the model, total vehicle mass M is considered to be equally distributed amongst four wheels with each wheel carrying an equivalent mass of $M/4$. Linear speed of the vehicle is denoted by V_t given by (2-5). Wheels have linear speed denoted by V_{w1} ($r\omega_{rm}$ of wheel 1) and V_{w2} ($r\omega_{rm}$ of wheel 2) given by (2-7) with a total adhesion of μ_{w1} and μ_{w2}, respectively. Therefore, each driving wheel contributes a tractive force defined by (2-9) with the total tractive effort given by

$$F_m = \mu_{w1}(v_{slip}^{w1})M_{w1}g + \mu_{w2}(v_{slip}^{w2})M_{w2}g, \tag{2-12}$$

where slip velocities are defined by

$$\begin{aligned} v_{slip}^{w1} &= v_{w1} - v_t = r\omega_{rm}^{w1} - v_t \\ v_{slip}^{w2} &= v_{w2} - v_t = r\omega_{rm}^{w2} - v_t, \end{aligned} \tag{2-13}$$

and the coefficients of friction are given by (2-10).

2.4 Electric Vehicle Propulsion System Model

Model of the propulsion system composed of electrical and mechanical subsystems have been implemented in MATLAB Simulink [22]. Block diagram of the combined model is illustrated in Figure 2.8. As can be seen in Figure 2.8, BLDC motors are driven by voltage-source-inverters controlled by Hall signals. Motors track reference speed of the vehicle provided by user through a PI controller. Parameters of the controller are tuned using the detailed model to achieve desired performance and acceptable tracking. Similar Hall-sensor based controllers have also been presented in [31]-[37].

The proposed controller block shown in Figure 2.8 will be introduced in Chapter 3. General idea here is to feed Hall signals through the controller and run both motors with a single set of Hall signals when the controller is activated. Otherwise, motors will operate with their respective signals and load experienced by one motor will be only slightly felt by the other motor due to change in speed of the entire vehicle and the running resistance. Developed model of the vehicle propulsion system will be utilized in the next chapter to evaluate various approaches for synchronizing and locking of independent driving wheels.

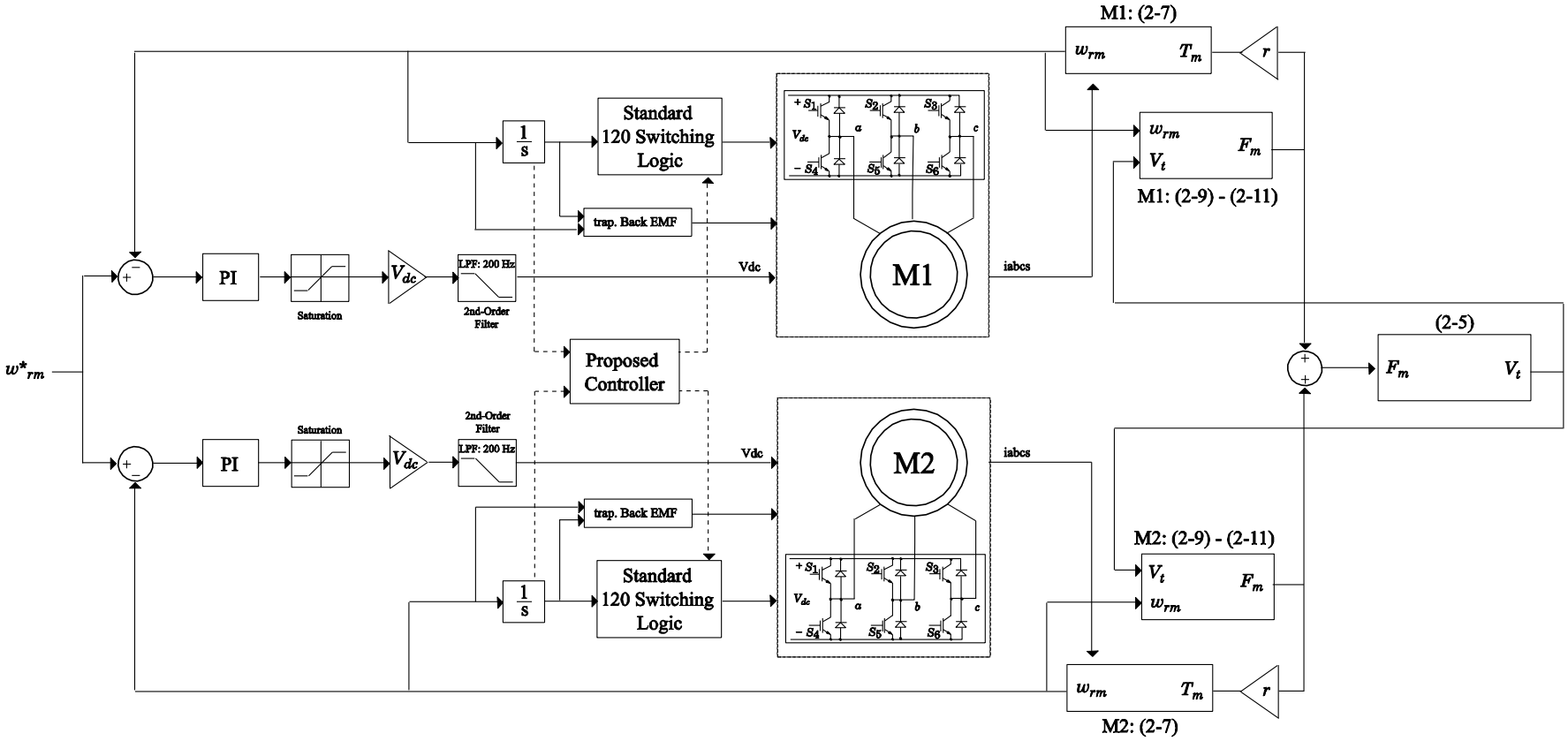

Figure 2.8 Block diagram of the electric vehicle propulsion system model composed of the electrical model of the BLDC motor-drive system and mechanical dynamics of the vehicle and wheels.

3 DETAILED MODEL AND SIMULATION OF LOCKING ELECTRIC DIFFERENTIAL SYSTEM

3.1 Introduction

Given considered electric vehicle configuration, an additional supervisory controller is needed to lock/synchronize wheels of the vehicle as there is no direct mechanical connection between the moving wheels [2]. This synchronization and locking of wheels, means that the controller is required to control both speed and relative positions of the motors (wheels) as shown in Figure 2.1. Primary objective of such controller is to emulate operation of a simple mechanical shaft whereby positions of the wheels are locked together and forced to operate at a constant relative position. This locking of wheels is also desirable under certain driving conditions to improve stability of the vehicle [17]. In addition, controller is also required to facilitate different speeds for the wheels needed for stable and soft cornering which in a typical vehicle is handled by a mechanical differential system. In this Chapter, we propose a Sync-Lock Controller that enables locking of the electrical differential system by processing Hall signals of the motors as shown in Figure 3.1. A detailed switch-level model of the EDS embedded with proposed SLC has been integrated with detailed model of the BLDC propulsion system developed in MATLAB Simulink as described in Chapter 2. Feasibility and the effectiveness of the proposed system will be demonstrated by a series of case studies. Proposed SLC method is also compared to a conventional method of synchronization and locking the BLDC motors using PI control loops.

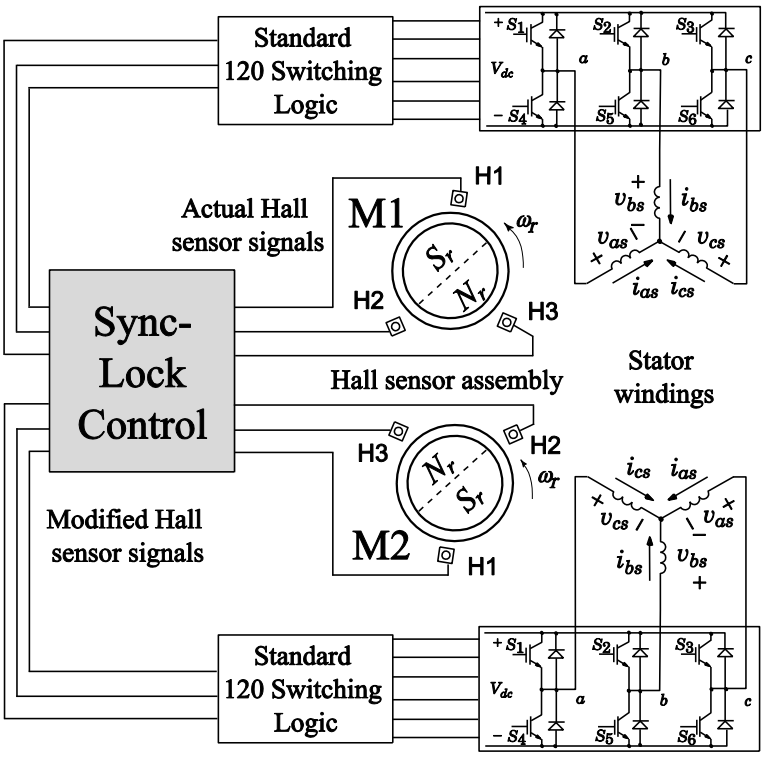

Figure 3.1 BLDC motor-drive system with the proposed Sync-Lock Controller.

3.2 Synchronization and Locking Techniques

3.2.1 Conventional Speed Control

Conventionally, speed of BLDC motors is controlled via external speed control loops. Hall sensors supply information about position of the rotor and speed for each motor independently. There have been a number of recently proposed control schemes that rely on Hall-sensor-based position and speed estimation [31]–[37]. In this type of controller, if speed of the motor drops because of an increase in load torque, speed error increases, which in turn increases effective dc voltage that feeds the machine by means of conventional pulse width modulation (PWM). The two motors therefore can be coupled with identical reference speeds on corresponding control systems as shown in Figure 3.2 [38]. Mechanical block, i.e. vehicle body, is the only indirect link between the two motors. This conventional approach results in soft locking of the EDS, which does not enforce same position of the rotors/wheels. Therefore, load experienced by one motor is only slightly felt by the other motor due to change in the speed of the entire vehicle and the running resistance. Extending this approach to position of the wheels would require

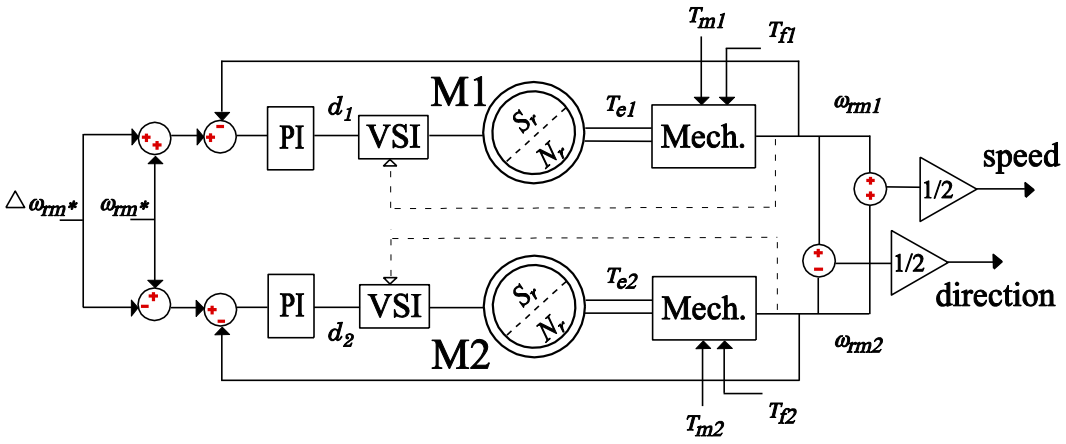

Figure 3.2 Conventional EDS speed control using PI loops.

special position encoders, which are expensive and would not be practical for vehicular applications where cost and minimal use of additional measuring sensors are very important.

3.2.2 Proposed Sync-Lock Control

Proposed Sync-Lock Control strategy synchronizes BLDC motors via corresponding Hall sensor signals as depicted in Figure 3.3. Proposed filtering technique is based on the idea of driving both motors with a common set of "averaged" signals, thereby locking speed and angle of both motors. Proposed locking strategy is different from a soft lock approach based on a PI controller as the two motors are locked internally by coupling respective magnetic fields through Hall sensor signals.

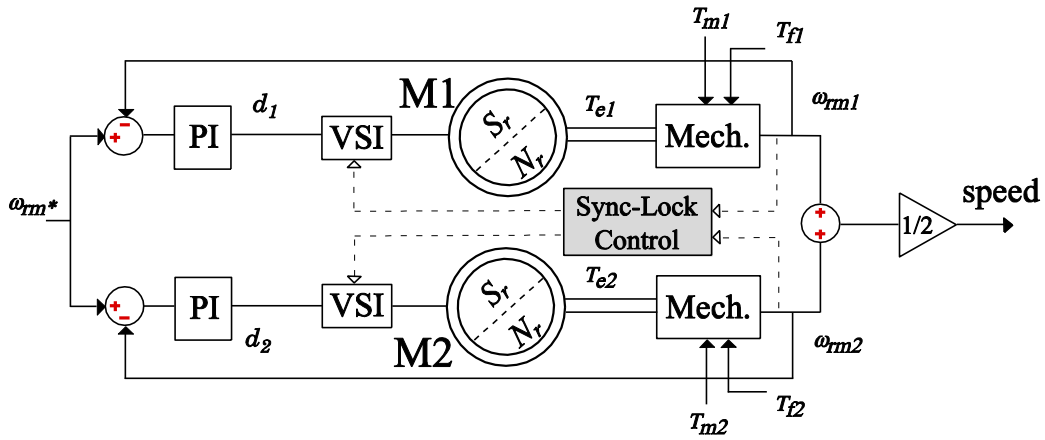

Figure 3.3 EDS speed control with the proposed SLC.

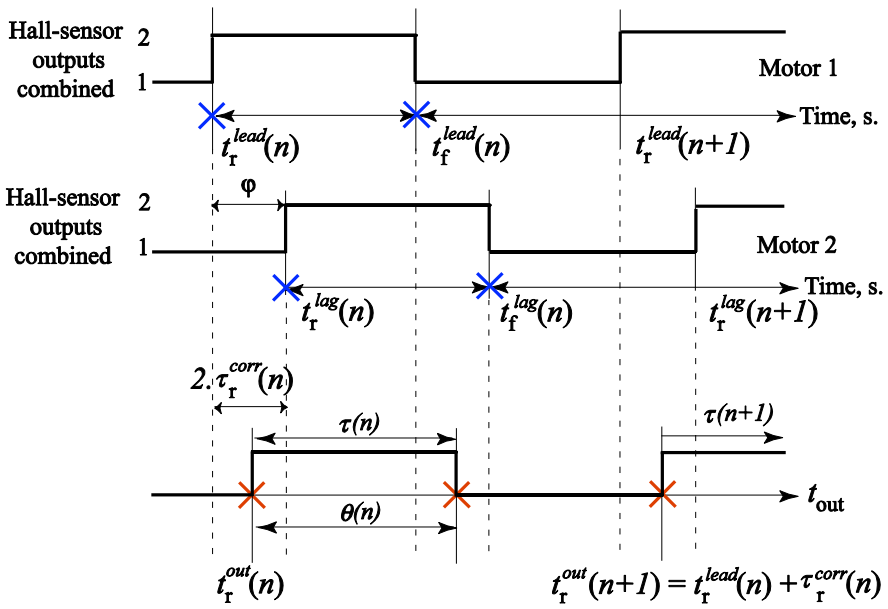

Figure 3.4 Proposed averaging of the Hall sensor signals for the SLC.

To better understand how to filter Hall-sensor signals, it is instructive to consider the diagram depicted in Figure 3.4. When the motor is running, Hall sensors produce square wave signals displaced by exactly 120 electrical degrees relative to each other. Output state of each Hall sensor as a function of rotor position is defined in Table 3.1. Combining all three outputs produces a square wave (see Figure 3.4, top first and second signals) with a period equal to one-third (60 electrical degrees) of a Hall-sensor period (180 electrical degrees).

The angular intervals between two successive switching events are denoted by $\theta(n)$. Durations of intervals $\theta(n)$ are denoted here by $\tau(n)$. Here, the angle φ denotes a possible delay or advance between rotors of the two motors [3]. These signals are used by inverter to provide the stator with desired voltages. Switching logic of the transistors in inverter is summarized in Table 3.2. Transistor numbers in this Table correspond to what is shown in Figure 3.1.

Table 3.1 Hall sensor states as a function of rotor position

H_1 on	$-90-\phi \le \theta_r \le 90-\phi$
H_2 on	$30-\phi \le \theta_r \le 210-\phi$
H_3 on	$150-\phi \le \theta_r \le 330-\phi$

Table 3.2 Standard switching intervals of a 120-degree inverter

Switching interval	Rotor position	Transistors on
1	$-30-\phi \le \theta_r \le 30-\phi$	5,1
2	$30-\phi \le \theta_r \le 90-\phi$	1,6
3	$90-\phi \le \theta_r \le 150-\phi$	6,2
4	$150-\phi \le \theta_r \le 210-\phi$	2,4
5	$210-\phi \le \theta_r \le 270-\phi$	4,3
6	$270-\phi \le \theta_r \le 330-\phi$	3,5

The SLC is based on constructing one set of Hall signals by appropriately modifying (averaging) signals from the actual sensors $H_{M1}\{1,2,3\}$ and $H_{M2}\{1,2,3\}$, respectively. Proposed method works by first finding the rising edge correction interval $\tau_r^{corr}(n)$ by means of averaging switching times $t(n)$ as follows:

$$\tau_r^{corr}(n)=\frac{1}{2}\left(t_r^{lag}(n)-t_r^{lead}(n)\right) \tag{3-11}$$

Once the correction value $\tau_r^{corr}(n)$ is established, actual timing for commutating the inverter transistors for next cycle can be found as follows:

$$t_r^{out}(n+1)=t_r^{lead}(n+1)+\tau_r^{corr}(n), \tag{3-12}$$

where $t_r^{lead}(n)$, the leading motors switching time, is defined as reference switching time of the system. Based on (3-11) and (3-12), period of the average signal can be calculated as

$$\tau(n+1)=1/2\left(\left(t_f^{lead}(n)-t_r^{lead}(n)\right)+\left(t_f^{lag}(n)-t_r^{lag}(n)\right)\right) \tag{3-13}$$

In general, the proposed SLC can be implemented using either an analog method (which is based on combination of logic gates, integrators, and a flip flop) or a digital method (which is based on a programmable integrated circuit microcontroller and digital signal processing). These approaches are briefly described below:

Analog Method

Analog implementation of the SLC is based on logic gates for processing signals, integrals for time measurements, sample and hold block for memory, and a flip flop as shown in Figure 3.5. Details of the timing signals in analog approach are shown in Figure 3.6. According to this implementation, the averaging is based on four basic operations: 1) time difference between the two signals is calculated by integrating XOR of the two signals and sampling the integrated signal (i.e. time difference) at falling edge of [H1 (NAND) H2]; 2) an OR gate along with an integrator is used to set up a time reference which is compared to half of time difference in step (1) to set the flip flop; 3) average period of the two signals is calculated by integrating algebraic sum of the two signals and sampling half of the result at falling edge of [H1 (OR) H2]; and 4), finally, period of the output signal is compared to average period of step (3) to trigger the reset of flip flop.

Proposed analog implementation of SLC averages combined signals and creates a new set of averaged signals that is used to control the inverters. Average signal essentially delays leading motor and advances lagging motor, and therefore locking the two wheels. It should be mentioned that the proposed implementation operates regardless of relative positions of the two motors and there is no need to distinguish (differentiate) leading and lagging motor.

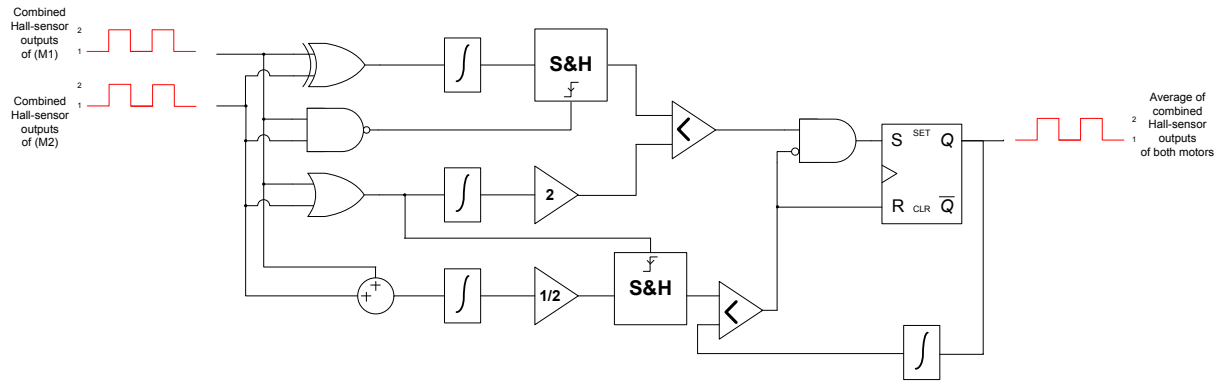

Figure 3.5 Analog implementation of the SLC that enables the timing of the input and output Hall signal transitions.

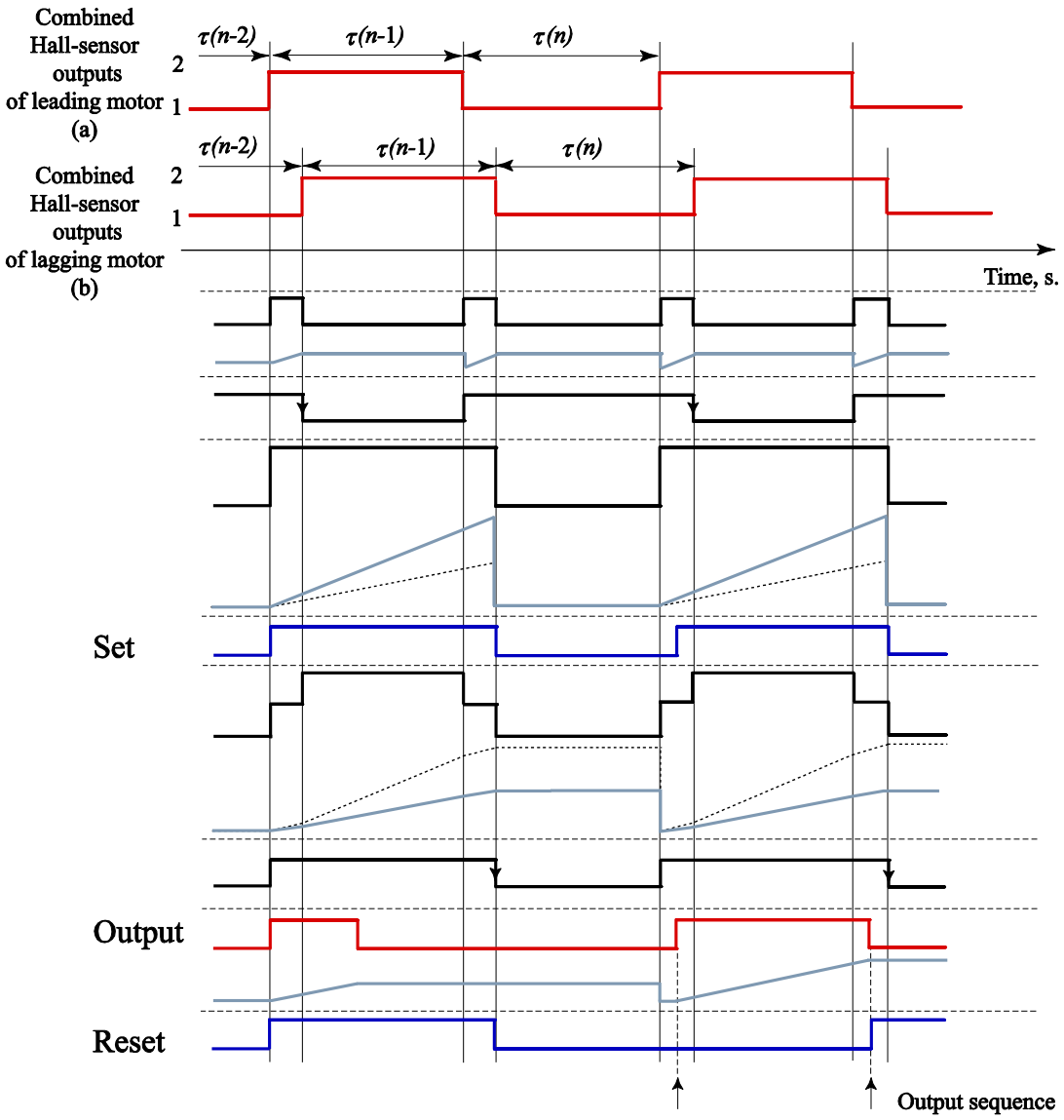

Figure 3.6 Timing of the input and output Hall signal transitions using the analog implementation of the proposed SLC.

Digital Method

Here we present a simple implementation of the SLC that can easily be used with existing drive systems. Proposed averaging algorithm is implemented using an interrupt-based approach that is suitable for digital signal processors (DSPs) or programmable microcontroller integrated circuits (PICs). The interrupt service routines (ISR) are triggered at switching points of the Hall signals. Here, each rising and falling edge ISR is considered to have a dedicated timer which is used to save last two time periods between the edges as shown in Figure 3.7. These time intervals are readily available simply as timer counts between Hall-sensor transitions. To run the motors with a single set Hall signals and switch transistors at the same time, output ISR needs to be invoked at a particular time to provide the inverters with modified Hall signals. With the latest time interval between interrupts denoted by τ_0, and the following one defined as τ_1, output interrupt is scheduled when $\tau_0 > \tau_1$, which is to be triggered after $\tau_1/2$ seconds. Same logic is used for averaging both rising and falling edges of the signals. It should be noted that in the proposed averaging technique there is no need to differentiate between leading and lagging motor, which makes this approach different from a master-slave configuration.

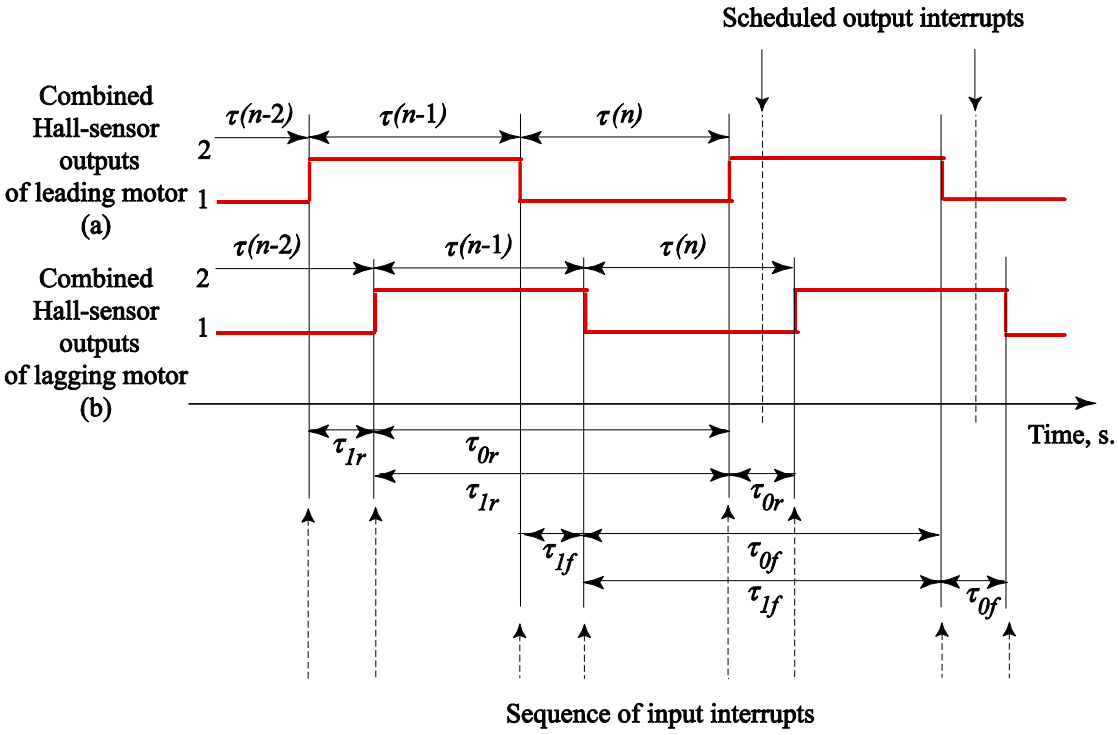

Figure 3.7 Timing of the input and output Hall signal transitions using the proposed digital implementation of the SLC.

3.3 Simulation Case Studies

In order to evaluate performance of the proposed SLC in simulation, detailed model has been developed and integrated with the model of EV developed in Chapter 2. Developed detailed model also included BLDC motor-drive system with the 120-degree inverter [27], [25], [9]. In following studies, the propulsion system is assumed to be supplied with $V_{dc} = 48V$. Coefficient, μ_0, of road surface friction defined by (2-10) is calculated with the parameters summarized in Table 2.1. Motion equations (2-5) and (2-7) are then determined by obtaining drive force, F_m defined by (2-9). PI controllers of the system have been tuned to achieve a satisfactory acceleration at start up. Same controller coefficients are used for differential system with conventional and proposed synchronization approaches. The corresponding controller coefficients along with vehicle mechanical parameters are summarized in Appendix A.

3.3.1 Sync-Lock Controller Transient

To illustrate enabling of the proposed locking mechanism, the two motors are initially assumed to be displaced by about 10 degrees. Then, the motors are commanded to speed up to 100 rad/s (about 955 rpm). After start up transient the motors settle down at 25 degrees apart. When SLC is enabled, the system undergoes a transient as depicted in Figure 3.8. This transient is due to initial angle difference of the motor shafts, which causes one of the motors to accelerate and another motor to decelerate to achieve desired locking. After that, both motors continue to operate at the same speed and angle synchronized as shown in Figure 3.8. Common speed shown in Figure 3.8 (top subplot) is the referred mechanical speed (in rpm) of virtual shaft driving the car forward. Slight difference in speed of the vehicle and the wheels is due to traction slip as discussed in Chapter 2, Section 2.3.1.

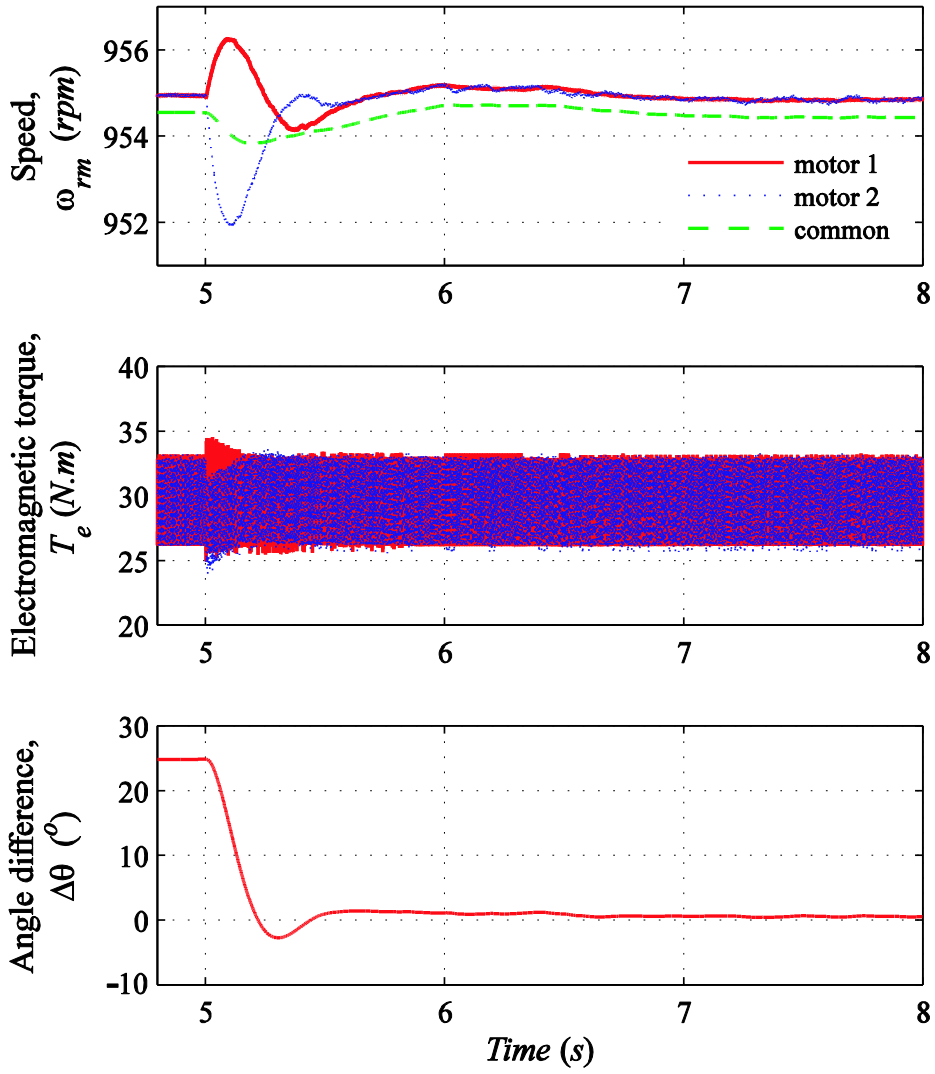

Figure 3.8 Simulated transient of the vehicular system when the proposed SLC is activated.

3.3.2 Load Step Transient

Here, performance of the locking mechanism is evaluated by subjecting the motors to a load disturbance. Figure 3.9 shows response of the EDS with conventional control. Figure 3.10 illustrates speeds and electromagnetic torques of the two motors when the proposed SLC is activated. Comparing Figure 3.9 and Figure 3.10, we can see that difference in speeds of the two motors is significantly reduced and improved with the proposed approach. To see the improvement more clearly, Figure 3.11 shows angle difference between the motors' shafts. As it can be seen in Figure 3.9 and Figure 3.10, conventional synchronization of the EDS, although achieves the same speed, leads to significant angle difference between shafts, which in a sense can be described as a "soft" synchronization. At the same time, the proposed SLC keeps the motor shafts aligned relative to each other as is desired.

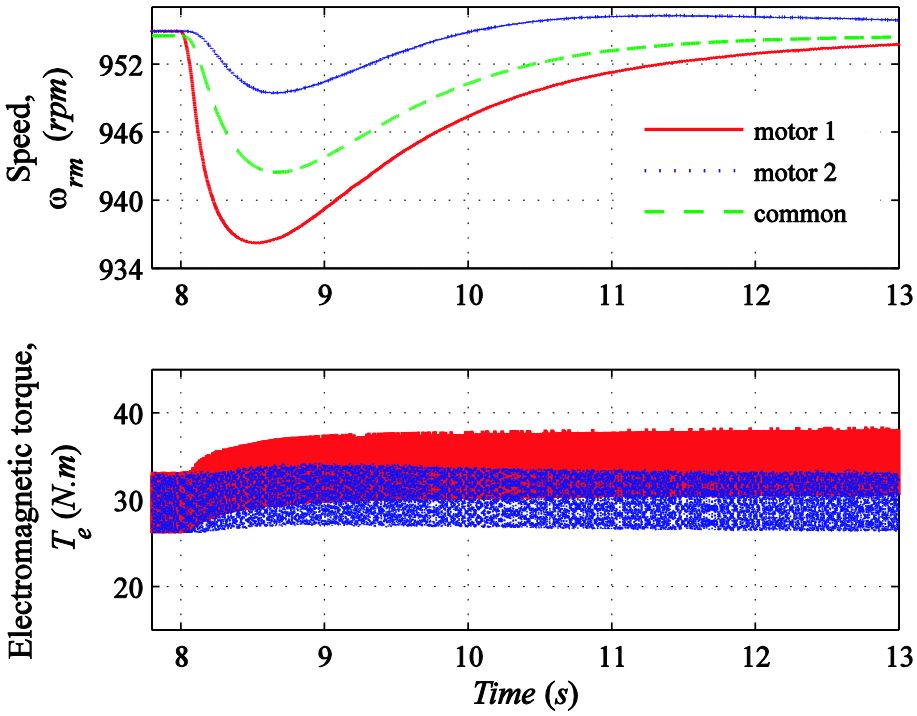

Figure 3.9 Speed and electromagnetic torque transient response due to load change when the EDS uses with conventional control.

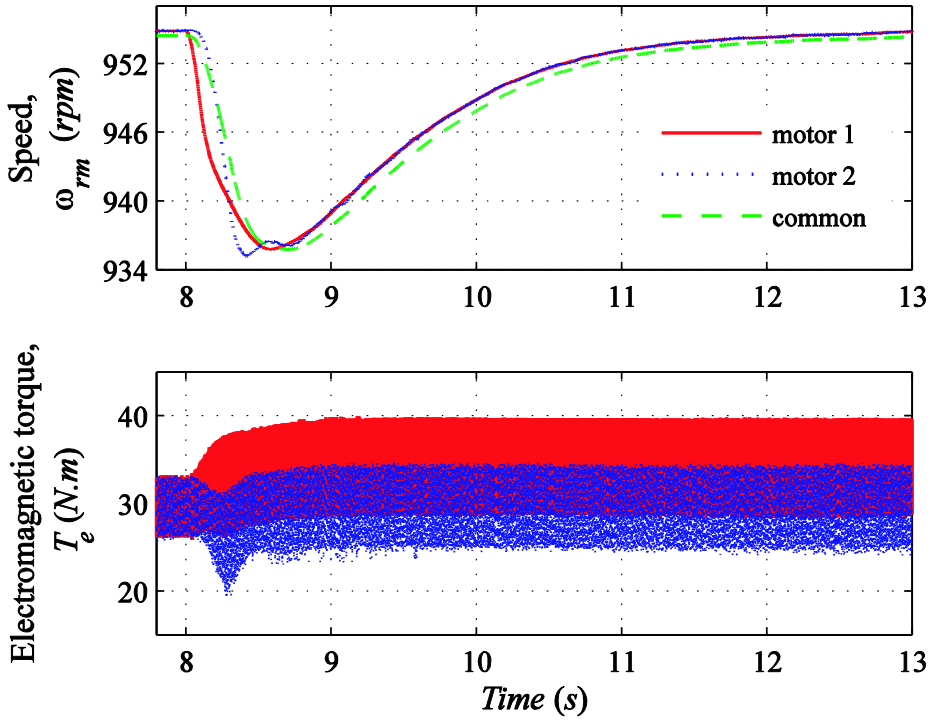

Figure 3.10 Speed and electromagnetic torque transient response due to load change when the EDS uses proposed SLC.

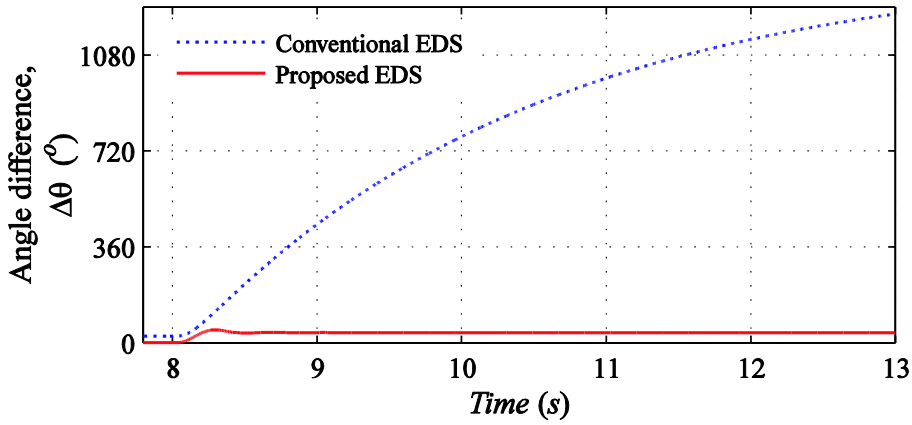

Figure 3.11 Difference in motor shafts angles using conventional and proposed synchronization approaches.

3.3.3 Emulated Driving Condition

To demonstrate motor drive system operation under uneven road conditions, in this subsection the system is subjected to a torque load profile that is different for the two subject wheels as shown in Figure 3.12 (top). This torque profile is considered to emulate a bumpy road condition that imposes different stresses on the vehicle's wheels. As can be seen in Figure 3.12 (second subplot), there is a significant difference in instantaneous speed of the shafts (wheels) when the EDS uses conventional synchronization control method. This is also observed in Figure 3.12 (fourth subplot), which shows the difference between shafts' angles. However, the proposed SLC achieves very good locking of the shafts and the speeds as depicted in Figure 3.12 (third and fourth subplots).

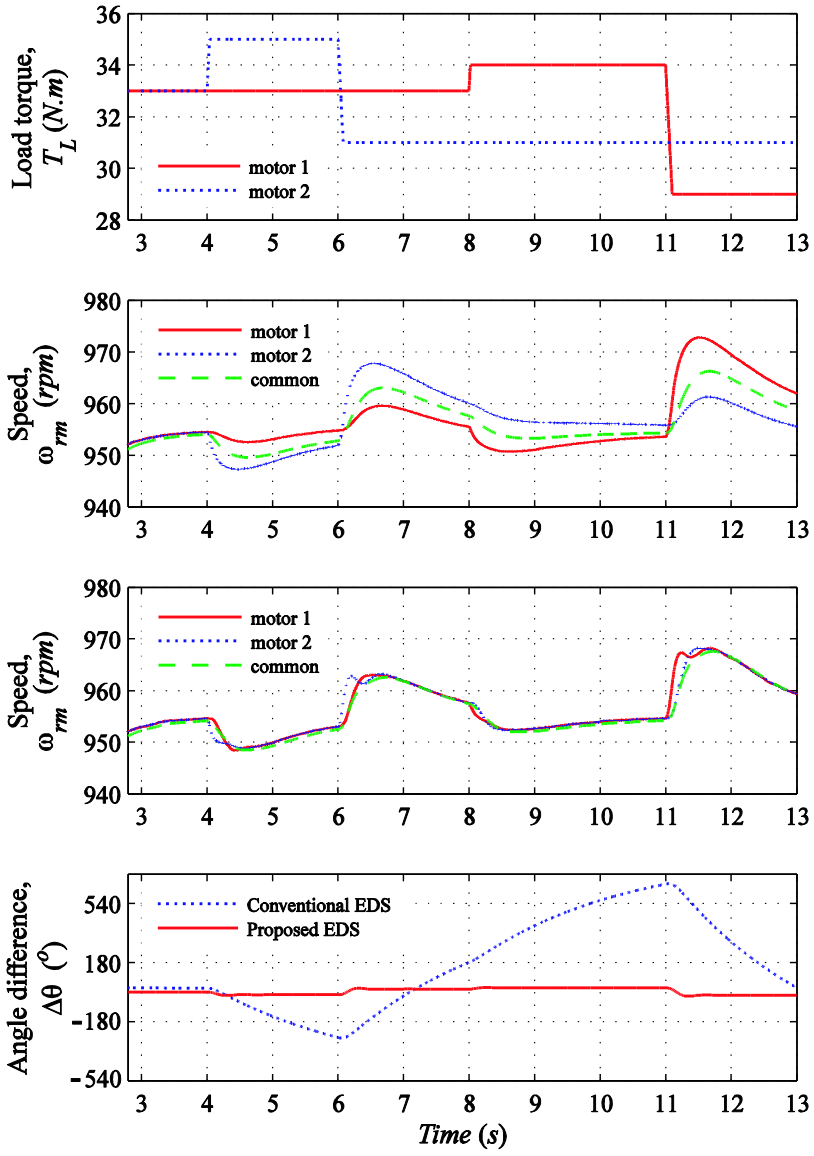

Figure 3.12 System response to emulated bumpy road when EDS uses conventional and proposed SLC control.

4 IMPLEMENTATION FOR LOW PRECISION BRUSHLESS DC MOTORS

4.1 Introduction

In a typical design configuration of BLDC machines, Hall sensors are mounted on a printed circuit board (PCB) attached to rear end of the motor [e.g. see Figure 1.3b)]. For a two pole machine, Hall sensors must ideally be placed exactly 120 degrees apart to produce control signals necessary for the standard 120-degree switching logic to control the six-step voltage-source inverter [27], [25], and [9]. If this is true, then Hall sensor signals will have consecutive transitions spaced out by exactly 60 electrical degrees. Although this is a common assumption in most literature sources, this condition is difficult to achieve in practice particularly in many mass-produced low-cost vehicular-type motors due to manufacturing tolerances. Therefore, to utilize Hall sensor signals for control purpose, these signals have to be filtered first to mitigate the errors [24], [19]-[21].

In this Chapter, we propose a digital implementation of the SLC for EV applications that takes into account Hall sensor misalignments. The implementation is based on typical three-phase BLDC motors [17] as shown in Figure 4.1, where we consider two propulsion motors to demonstrate the proposed concept. Aforementioned filtering and locking algorithm SLC is then applied directly to the original Hall sensor signals to produce a modified set of signals that are used to the drive both inverters as depicted in Figure 4.1.

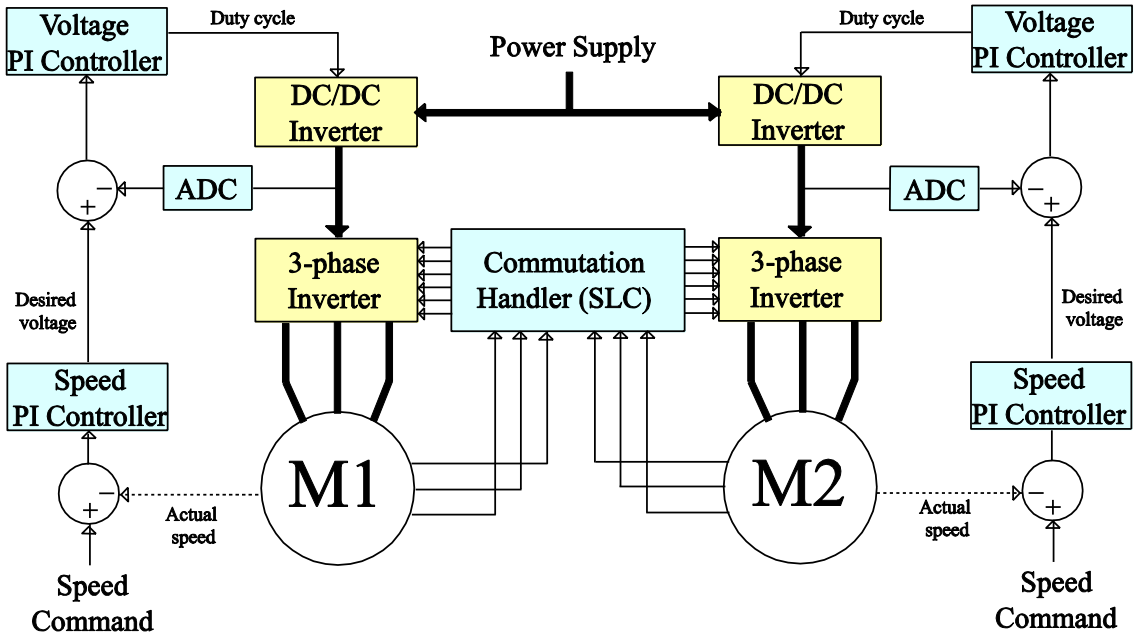

Figure 4.1 Proposed two-BLDC motor-drive vehicular propulsion system.

4.2 Brushless DC Motors with Unbalanced Hall-Sensors

The poorly aligned Hall sensors are actually quite common in low-cost mass-produced BLDC motors as has been described in literature [19]-[21], [24]. Since such low-cost motors are very likely to be found in vehicular applications, this phenomenon has to be considered for the purpose of this thesis as well. Figure 4.2 depicts phase currents of our sample prototype motors with the parameters summarized in Appendix B. Here, the angular- and time-duration between each subsequent Hall sensor transition is denoted by $\theta(n)$ and $\tau(n)$, respectively, and n denotes the interval number. In case of a BLDC motor with ideally-placed Hall sensors, angular duration $\theta(n)$ between subsequent Hall sensor transitions should be 60 degrees for all n, which is clearly not true in Figure 4.2. Also, in steady state operation, time intervals $\tau(n)$ should be equal. Such unbalanced conduction among the phases leads to increase in the torque ripple as has been shown in [24], and is therefore very undesirable.

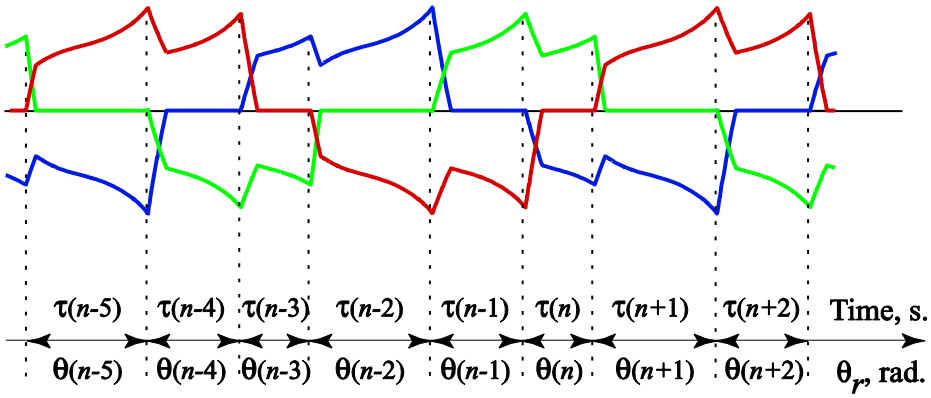

Figure 4.2 Stator currents with unequal conduction intervals due to Hall-sensor misalignment [24].

4.2.1 Filtering Hall-Sensor Signals

Frequency content of the sequence $\tau(n)$ introduced in Figure 4.2 can be evaluated by using discrete-time Fourier series (DTFS) [39]. Based on that, the sequence $\tau(n)$ can be written as:

$$\tau(n) = \sum_{k=0}^{N-1} c_k e^{j2\pi kn/N} \qquad (4\text{-}1)$$

where the Fourier coefficients $\{c_k\}$, $k = 0,1,...,N-1$, provide description of $\tau(n)$ in frequency domain. In our case, the signal $\tau(n)$ has one zero-frequency component and two components with frequencies of $\frac{2\pi}{3}$ and $\frac{4\pi}{3}$ radians per sample [24].

Purpose of filtering schemes presented in this section is to make the sequence of time intervals follow that of a motor with perfectly positioned Hall sensors. To achieve this, filter must remove $\frac{2\pi}{3}$ and $\frac{4\pi}{3}$ harmonics from the sequence $\tau(n)$ which can be done with selection of linear filters that generally have the following form:

$$\bar{\tau}(n) = \sum_{m=1}^{M} b_m \tau(n-m) \tag{4-2}$$

where M is the order of the filter corresponding to number of time intervals taken into account, and b_m is weighting coefficient that depends on a particular filter realization.

Different linear filters were proposed in [24] including 3-step averaging; 6-step averaging; linear extrapolating-plus-averaging; and quadratic extrapolating-plus-averaging. The final equations produced for these averaging filters are denoted by $\bar{\tau}_{a3}$, $\bar{\tau}_{a6}$, $\bar{\tau}_l$ and $\bar{\tau}_q$, respectively. The equations are presented here for completeness.

$$\bar{\tau}_{a3}(n) = \frac{1}{3}\left(\tau(n-1) + \tau(n-2) + \tau(n-3)\right) \tag{4-3}$$

$$\bar{\tau}_{a6}(n) = \frac{1}{6}\left(\tau(n-1) + \tau(n-2) + \tau(n-3) + \tau(n-4) + \tau(n-5) + \tau(n-6)\right) \tag{4-4}$$

$$\bar{\tau}_l(n) = \frac{1}{3}\left(2\tau(n-1) + \tau(n-2) + \tau(n-3) - \tau(n-4)\right) \tag{4-5}$$

$$\bar{\tau}_q(n) = \frac{1}{3}\left(3\tau(n-1) + \tau(n-3) - 2\tau(n-4) + \tau(n-5)\right) \tag{4-6}$$

Depending on characteristics of the available BLDC motors and requirements for dynamic performance of the vehicular propulsion system, any one of the filters (4-3) - (4-6) may be considered in combination with the synchronization approach developed in this thesis.

4.3 Implementation of SLC with Correction for Hall Sensor Misalignment

The proposed Sync-Lock Control strategy synchronizes BLDC motors via corresponding Hall sensor signals as depicted in Figure 4.1. However, to apply this locking technique effectively, the errors due to Hall sensor misalignment must be removed first. Filter [24] is considered here to mitigate inaccurate positioning of the Hall sensors.

4.3.1 Digital Implementation of Hall-Sensor Signals Filtering

Proposed filtering algorithm can be readily implemented on a dsPIC microcontroller using the so-called software interrupt service routines (ISR). Using this method, switching of Hall sensors triggers the input ISR, at which time all necessary calculations (instructions) are done inside the microcontroller. With dedicated timers for the rising and falling edges, continuous operation of drive is enabled by resetting internal time counter of the microcontroller back to zero at either rising or falling edges of input signals. Hence, time intervals $\tau(n)$ are readily available simply as the timer counts between rising and falling edges of Hall-sensor signals. To switch transistors when the filter is enabled, software output ISR has to be invoked at a particular time to provide the inverter with modified Hall signals. This time of the next switching may be expressed as

$$t_{next\_sw} = \bar{t}(n) + \bar{\tau}(n) = t_{out}(n+1) \tag{4-7}$$

where $\bar{\tau}(n)$ denotes averaged time interval as calculated using any of the filters (4-3)–(4-6), and $\bar{t}(n)$ is the so-called reference switching time as defined in [24]. Also, here $t_{out}(n+1)$ refers to the time when the modified output Hall signals will be switched.

In order to minimize computational resources, a direct implementation of (4-7) cannot be considered as it requires continuous calculation of both the reference time $\bar{t}(n)$ and the averaged interval $\bar{\tau}(n)$. For an efficient implementation of (4-7), we need to relate the time $t_{out}(n+1)$ (when the modified output Hall signals will be switched) to the time when original Hall signal has triggered the input ISR. Denoting most-recent calling of the input ISR by $t_{in}(n)$, time of the next output ISR can be expressed as:

$$t_{out}(n+1) = t_{in}(n) + \tau^{corr}(n) \tag{4-8}$$

where $\tau^{corr}(n)$ is the appropriate correction term. Equation (4-8) is very straightforward and computationally efficient as it requires a simple scheduling of the output ISR by offset correction time

$\tau^{corr}(n)$ without the need for reference time as in (4-7). In this implementation, the output ISR is scheduled by simply comparing value of the timer and correction term.

Calculation of correction time $\tau^{corr}(n)$ is best understood by considering Figure 4.3. The bottom axis in Figure 4.3 depicts the input interrupts that are triggered by actual Hall sensor signals, $t_{in}(n)$. The scheduled output software interrupts for modified switching signals are depicted on the top axis, $t_{out}(n)$. Assuming a certain reference time $\bar{t}(n)$ and a given $\bar{\tau}(n)$, the correction term is calculated using (4-1)–(4-2) as

$$\tau^{corr}(n) = t_{out}(n+1) - t_{in}(n) = \bar{t}(n) + \bar{\tau}(n) - t_{in}(n). \tag{4-9}$$

Computation of (4-9) requires knowledge of the reference time. This time may be obtained by averaging switching times of the three phases as depicted in Figure 4.3.

$$\bar{t}(n) = \frac{1}{3}\left(t(n) + t'(n) + t''(n)\right) \tag{4-10}$$

Here, $t(n)$ is time of the last switching of input Hall signal, and $t'(n)$ and $t''(n)$ are the times extrapolated from the two preceding input Hall signal transition times, as follows:

$$\begin{aligned} t'(n) &= t_{in}(n-1) + \bar{\tau}(n) \\ t''(n) &= t_{in}(n-2) + 2\bar{\tau}(n) \end{aligned} \tag{4-11}$$

As can be seen in Figure 4.3, the most recent input interrupt has occurred at $t_{in}(n)$. Last two input interrupts have occurred at $t_{in}(n-1)$ and $t_{in}(n-2)$ respectively. These times are used to calculate extrapolated terms according to (4-11), and then the reference time according to (4-10).

Combining the results, reference time is calculated in terms of input interrupts as:

$$\bar{t}(n) = \frac{1}{3}\left(t_{in}(n) + t_{in}(n-1) + t_{in}(n-2)\right) + \bar{\tau}(n) \tag{4-12}$$

Since $t_{in}(n-1)$ and $t_{in}(n-2)$ refer to the previous input interrupt times, they can be expressed as:

$$t_{in}(n-1) = t_{in}(n) - \tau(n-1) \tag{4-13}$$

$$t_{in}(n-2) = t_{in}(n) - \tau(n-2) - \tau(n-1) \tag{4-14}$$

Combining (4-12)–(4-14) and (4-9), the correction term is represented as:

$$\tau^{corr}(n) = \frac{1}{3}(-2\tau(n-1) - \tau(n-2)) + 2\bar{\tau}(n) \tag{4-15}$$

Correction term $\tau^{corr}(n)$ can now be used for whole range of different filters presented in [24], [19], and [20] by substituting the appropriate expression for $\bar{\tau}(n)$. After all relevant substitutions and grouping of terms, the final correction terms for each filters (4-3)–(4-6) can be expressed as:

$$\tau_{a3}^{corr}(n) = \frac{1}{3}(\tau(n-2) + 2\tau(n-3)) \tag{4-16}$$

$$\tau_{a6}^{corr}(n) = \frac{1}{3}(-\tau(n-1) + \tau(n-3) + \tau(n-4) + \tau(n-5) + \tau(n-6)) \tag{4-17}$$

$$\tau_{l}^{corr}(n) = \frac{1}{3}(2\tau(n-1) + \tau(n-2) + 2\tau(n-3) - 2\tau(n-4)) \tag{4-18}$$

$$\tau_{q}^{corr}(n) = \frac{1}{3}(4\tau(n-1) - \tau(n-2) + 2\tau(n-3) - 4\tau(n-4) + 2\tau(n-5)) \tag{4-19}$$

Without loss of generality, for purpose of this thesis, we consider third order filter (4-16) to prove the SLC concept, but the proposed algorithm can readily be extended for higher order filters. Thus, the third order filter will be implemented using (4-3) and (4-16) which is computationally efficient and simple compared to [24].

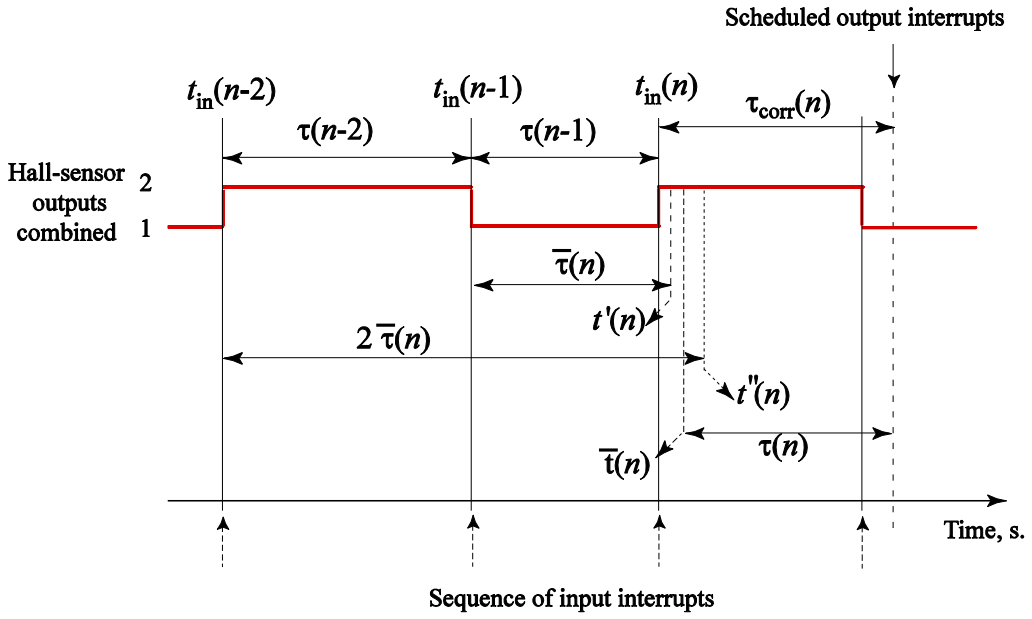

Figure 4.3 Timing of the input and output Hall signal transitions.

4.3.2 Implementation of Hall-Sensor Signals Locking

The SLC is based on constructing one set of Hall signals by appropriately modifying (filtering/averaging) the signals from actual sensors $H_{M1}\{1,2,3\}$ and $H_{M2}\{1,2,3\}$. Averaging is done by first finding the rising edge offset term which is

$$\tau_{dr}(n) = t_r^b(n) - t_r^a(n). \tag{4-20}$$

Once the offset value $\tau_{dr}(n)$ is established, actual timing for commutating the inverter transistors for next cycle can be found as follows:

$$t_r^{out}(n+1) = t_r^a(n+1) + (1/2)\tau_{dr}(n), \tag{4-21}$$

where $t_r^a(n)$, the leading motors switching time, is defined as reference switching time of the system. A similar approach is used for falling edges of the signals resulting in period of the average signal:

$$\tau(n+1) = \frac{1}{2}\left(\left(t_f^a(n) - t_r^a(n)\right) + \left(t_f^b(n) - t_r^b(n)\right)\right). \tag{4-22}$$

Averaging algorithm is also based on the software ISR triggered by rising and falling edges of the input signals. As before, for each rising and falling edge, the ISR has a dedicated timer which is used to save the last two time periods between the edges as shown in Figure 4.4. In this algorithm the latest time interval between interrupts is defined as τ_0, and the following one is defined as τ_1. The output interrupt is scheduled when $\tau_0 > \tau_1$ to be triggered after $\tau_1/2$ seconds. Same logic is used for averaging both rising and falling edges of the signals.

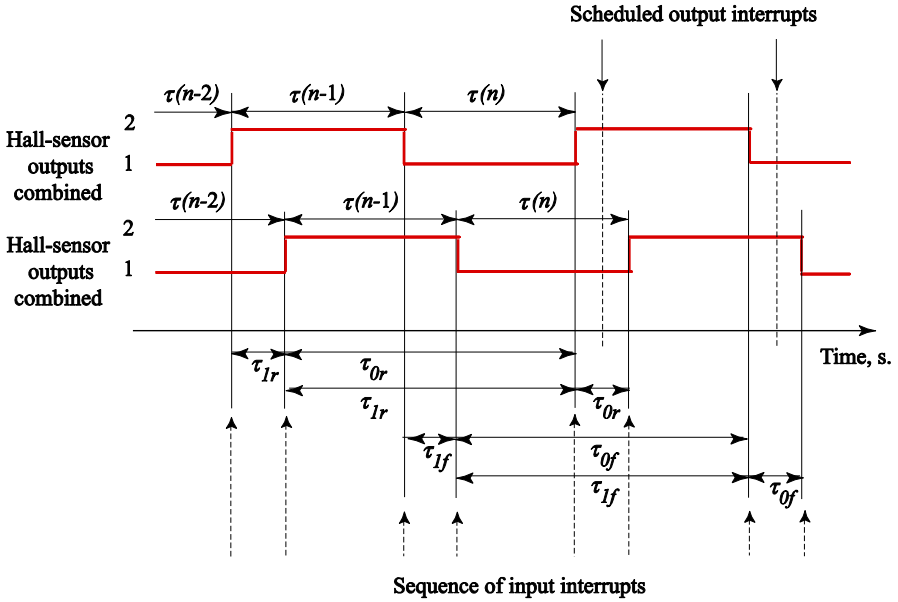

Figure 4.4 Timing of the input and output Hall signal transitions (averaging).

4.3.3 Combined Implementation of Filtering and Locking of Hall-Sensor Signals

It is essential to integrate the proposed techniques efficiently and minimize computational resources as much as possible. The proposed techniques are integrated using only two software ISRs with dedicated timers. One ISR and timer is devoted to rising edges of the input signals, while another ISR and timer pair is used for falling edges of the input signals. Finally, the third timer is utilized for scheduling output interrupt for both the rising and falling edges.

Proposed algorithm can be explained by considering rising and falling edges of Hall signals separately. Figure 4.5 illustrates timing of the rising edge interrupts. Output rising edge interrupt is scheduled at the input falling edge when $\tau_{0f} > \tau_{1f}$ to be triggered at $\tau_{corr}(n+2)+\tau_{dr}/2$, where τ_{dr} is the offset between two signals defined at rising edge when $\tau_{0r} < \tau_{1r}$. This offset can be calculated as follows

$$\tau_{dr} = \tau_{0r} + \left(\tau(n) - \tau_{corr}(n)\right)_a - \left(\tau(n) - \tau_{corr}(n)\right)_b. \qquad (4\text{-}23)$$

Here, subscript "*a*" denotes period difference of the leading motor; and subscript "*b*" is used to denote period difference of the lagging motor. It should be noted that either one of motors 1 and 2 could be leading or lagging.

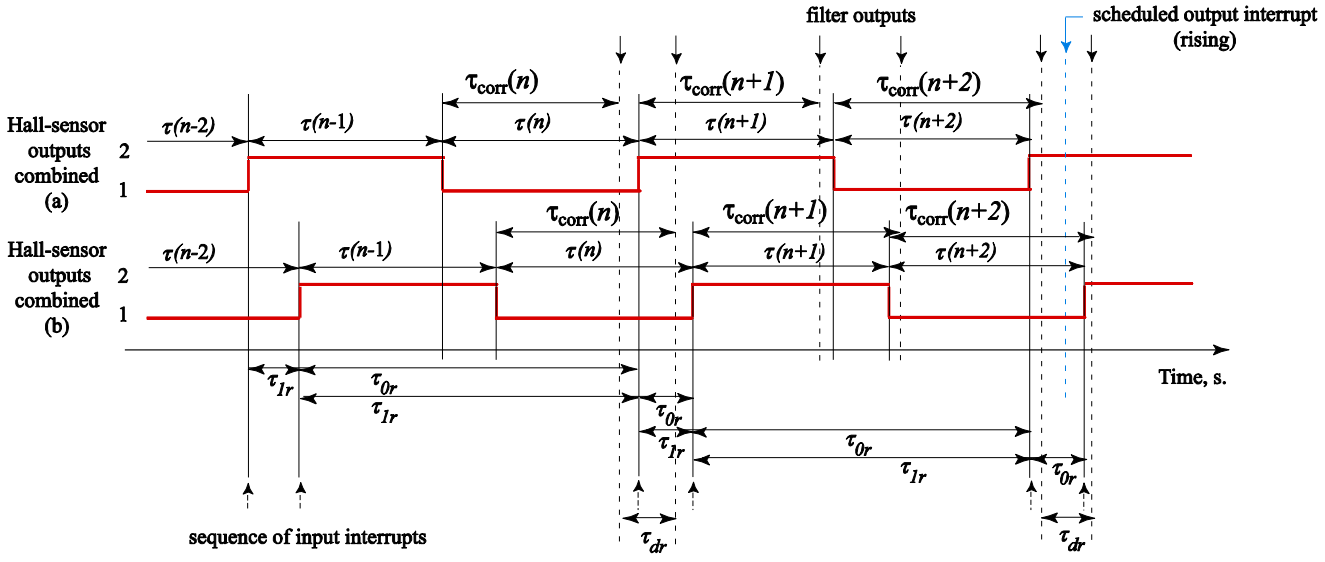

Figure 4.5 Timing of rising edge input and output interrupts.

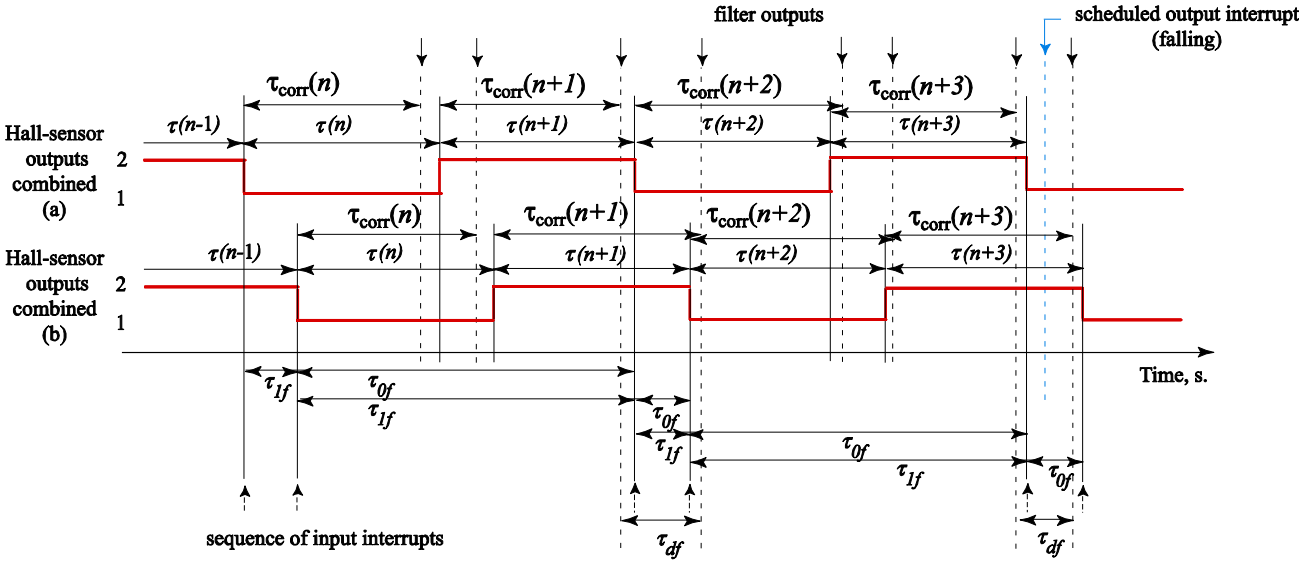

Figure 4.6 Timing of falling edge input and output interrupts.

Similar to the rising edge interrupt, the output falling edge interrupt is scheduled at input rising edge when $\tau_{0r} > \tau_{1r}$ to be triggered at $\tau_{corr}(n+3) + \tau_{df}/2$, where τ_{df} is the offset between two signals when $\tau_{0f} < \tau_{1f}$ which can be calculated as

$$\tau_{df} = \tau_{0f} + \left(\tau(n+1) - \tau_{corr}(n+1)\right)_a - \left(\tau(n+1) - \tau_{corr}(n+1)\right)_b. \qquad (4\text{-}24)$$

As shown in Figure 4.5 and Figure 4.6, offset between two filtered signals is implemented by taking into account the fact that filtered signal could be located before or after the actual input interrupt. Relative position of the filtered and actual signal depends on many conditions, e.g. relative position errors, whether the motor is decelerating or accelerating, etc. Finally, in both the rising and falling edge interrupts when output ISR is invoked, next state of the Hall sensors is predicted according to the existing state and the direction of rotation. After that, output Hall signals will be changed to switch inverters of the motors into their next topological state. With the proposed algorithm, closest two phases of two motors are averaged and locked together rather than the matching phases. This is desirable as the two motors may be locked together at any point during operation regardless of their relative positions.

5 HARDWARE REALIZATION USING PIC MICROCONTROLLER

5.1 Introduction

In this Chapter, we provide an efficient and robust algorithm to realize digital implementation of the EDS synchronization locking as described in Chapter 4. The proposed algorithm is developed on MPLAB® IDE v8.60 and programmed on a basic programmable integrated circuit microcontroller (dsPIC30f2020) [40] using MPLAB® ICD 3 In-Circuit Debugger System as shown in Figure 5.1. The controller is then evaluated using two BLDC motor-drive systems with each motor loaded by a dc machine dynamometer. Experimental system setup is illustrated in Figure 5.1. Detailed description of the developed algorithm along with experimental case studies is presented later in this chapter.

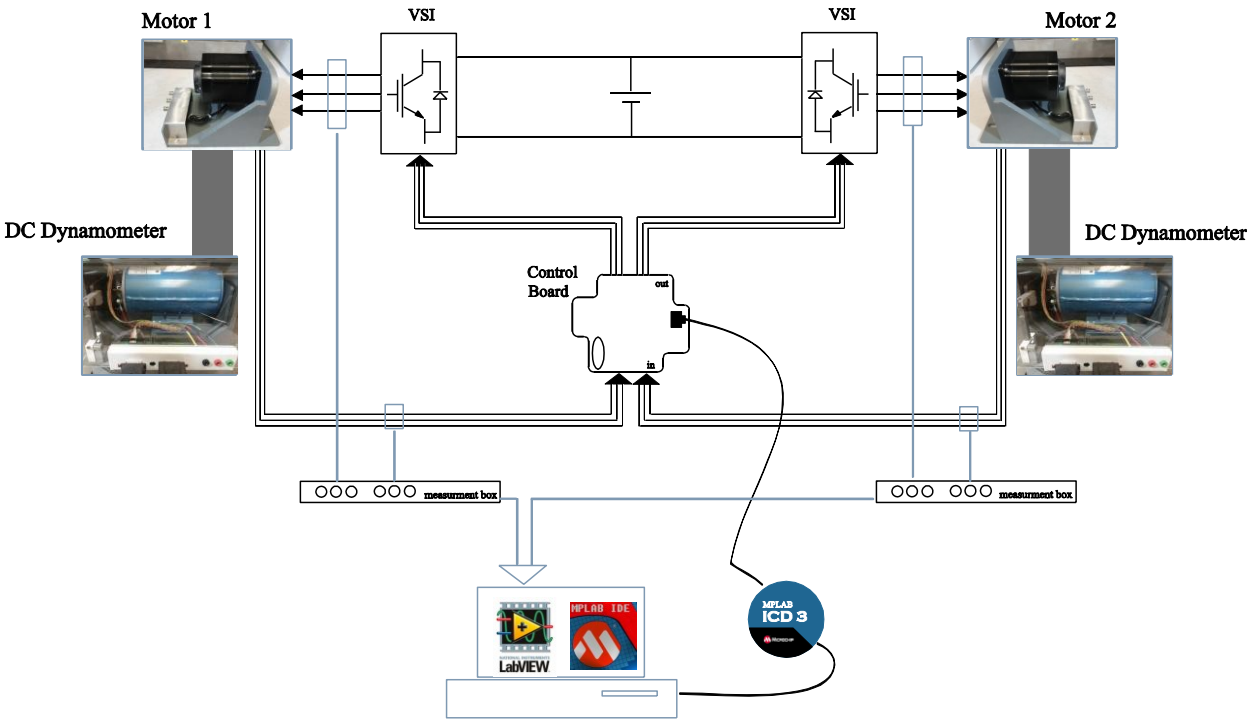

Figure 5.1 Experimental system setup.

5.2 Algorithm Implementation and Hardware Prototype

In order to have a robust and reliable SLC, we need to develop an algorithm that is able to handle special cases such as rapid acceleration/deceleration, overlap of Hall signals of two motors, overlap of filtered and actual Hall signals, lagging or leading filtered Hall signals, etc. This Section describes the developed controller algorithm and the hardware prototype that satisfies stated requirements.

5.2.1 Digital Implementation of EDS

Figure 5.2 illustrates a simplified flow chart of the developed algorithm based on ISRs. Program starts by initializing the appropriate registers of the microcontroller. The controller calculations are triggered with first detection of the input software interrupt (i.e. change in state of a Hall signal). Upon this detection, the ISR will be invoked and the microcontroller will become ready to perform SLC operations. Due to inherent memory of the proposed filtering and averaging technique, the controller output signal will not be available right away. As the proposed averaging technique requires just one operational cycle, the delay is dominated by order of the filter used in the system. Depending on order of the filter, a certain number of input interrupts must be detected to record sufficient number of time intervals for proper operation of the filter. Considering that minimum order of the proposed filter is three, there is no need to check if the averaging condition has been met during operation as filtering requirement guarantees proper operation of signal averaging.

As mentioned in previous Chapter, with one timer dedicated for rising edges and one for falling edges, the time interval between two edges of individual signals are recorded by reading the timer values at appropriate instances during the operation. After recording periods of the signals, filter conditions (i.e. not enough history terms, rapid acceleration/deceleration, deactivation of the filter by a manual switch, etc.) are verified as shown in Figure 5.2. If filtering conditions are not met, existing Hall signals are passed directly to the output for switching inverter transistors. In this case, the controller is effectively disabled and no output interrupts are scheduled. If filtering conditions are met for the first time, Hall signals are still shifted through to the output but output filter interrupt is enabled this time. In addition, the correction term is calculated and used for scheduling the filter output interrupt. If filtering conditions are met and it is not the first time, then two different operations need to be handled. One of the operations is dedicated to filtering Hall signals and another one is devoted to averaging of Hall signals from the two motors.

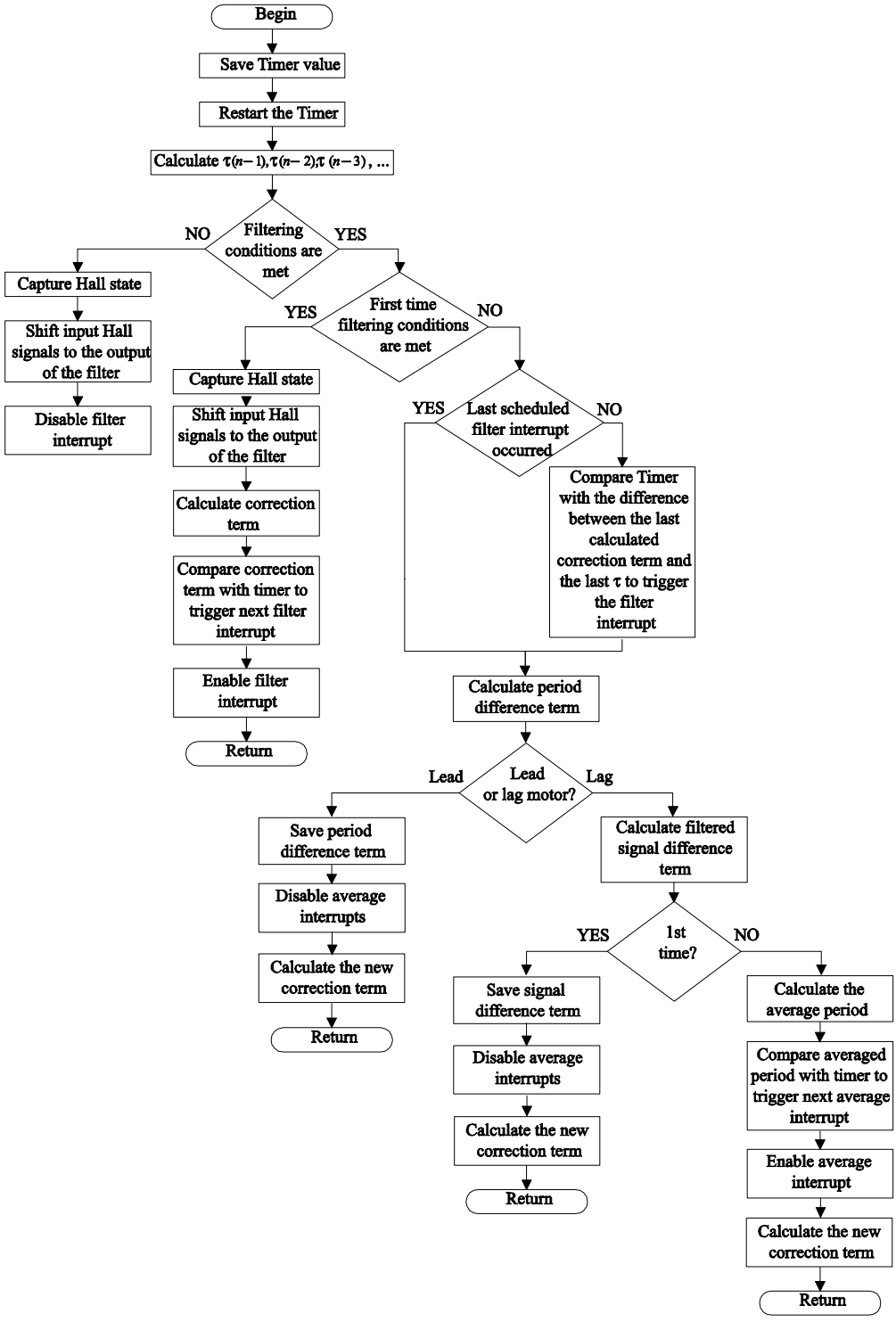

Figure 5.2 Flow chart of conditions and functions performed during input the ISR.

For filtering Hall signals, output filter interrupts may have to be switched before or after the next input interrupt (rising/falling edges) depending on many conditions. In first scenario, output software interrupt is invoked earlier making inverter switching happen before the actual Hall-sensor-signal-transition. This could happen for example when motor is under deceleration and/or when a given Hall sensor has an error in direction of rotation. Then, at the time of input ISR corresponding correction term $\tau^{corr}(n)$ is calculated and used to schedule the next output software interrupt to make the inverter switch. In second scenario, actual Hall sensor signal comes ahead of what it should be in an ideal case. This may happen when the motor is accelerating and/or when a given Hall sensor has an error in opposite direction to the motor rotation. If this case, at the time of input ISR, when timer is reset to zero, next output software interrupt will be scheduled for the time determined by the difference $\tau^{corr}(n-1)-\tau(n-1)$. In addition to this, another filter output interrupt for next switching interval should be scheduled as well. This is simply done by calculating new correction term $\tau^{corr}(n)$ and putting it as a second request for invoking the filter output interrupt.

For averaging Hall signals, in addition to period difference term, signal difference term (i.e. difference between the Hall signals of the two motors) is calculated. This term will only be available at the lagging signal interrupt. If it is the first time at lagging motor interrupt, the filtered Hall signals are just buffered through to the output but the output average interrupt is enabled. If it is not the first time at lagging motor interrupt, the average output interrupt is scheduled according to the signal difference term. Averaging of filtered Hall signals is also considered. Here, the two discussed scenarios (where the output filter interrupts may have to be switched before or after the next input interrupt) are taken care of inherently by defining the signal difference terms (4-23) and (4-24) with a positive leading motor period difference, $\left(\tau(n+1)-\tau_{corr}(n+1)\right)_a$; and a negative lagging motor period difference, $\left(\tau(n+1)-\tau_{corr}(n+1)\right)_b$.

The steps performed during the output ISR are shown in Figure 5.3. When the output ISR is invoked, next state of the Hall sensors is predicted according to existing state and direction of rotation of the two motors. Steps are the same for both filtering and averaging operations. It is just the matter of which state and at what point the inverter is switched. For filtering, the output Hall signals will be changed to switch the inverter into its next topological state. But for averaging, output Hall signal of the leading motor will be changed to switch the inverter into its current topological state while lagging motor will be changed to switch the inverter into its next topological state. After this point, all variables are updated and the output ISR is finished. The program then continues to run until next input interrupt is detected.

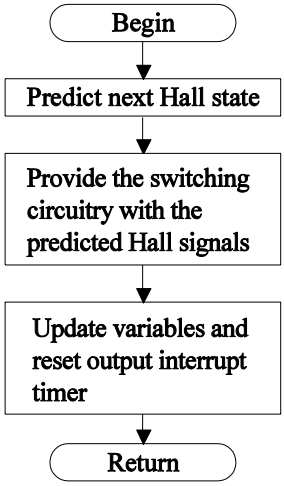

Figure 5.3 Flow chart of the software output ISR.

5.2.2 Hardware Prototype

The proposed Sync-Lock Controller has been realized on a basic programmable integrated circuit microcontroller (dsPIC30f2020) [40]. This and similar microcontrollers are often used in many inexpensive BLDC drive systems [41]. Figure 5.4 shows a simplified diagram of the SLC unit. The controller accepts original Hall sensor signals as an input (input Hall signals), and provides switching circuitry with modified signals (output Hall signals).

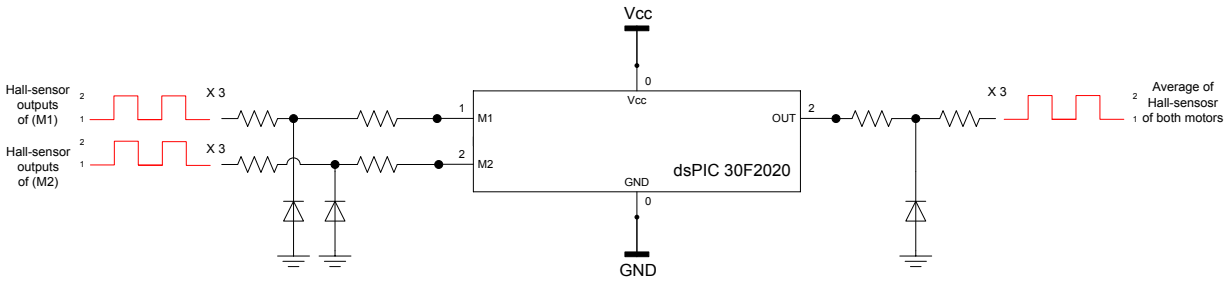

Figure 5.4 Input and output Hall signal transitions using the proposed averaging.

Actual printed circuit board of the prototype and its simplified schematic are shown in Figure 5.5 (a) and (b), respectively. Details of the PCB schematic and layout are summarized in Appendices C and D respectively. As shown in Figure 5.5, the prototype SLC dongle has several auxiliary components in addition to the microcontroller in order to make it operational for various BLDC motor drive systems.

The voltage regulator is designed to handle input voltages from 6 to 48 V_{dc}. In this arrangement, the dongle can be powered either from t dc bus of the BLDC motor drivers or directly from dc supply that feeds Hall sensors of the motor. Input and output ports of the microcontroller are also protected against accidental over-voltage. The microcontroller can be re-programmed with different filters through its data programming port, as well as enabled or disabled using manual switch. Potentially, the dongle can be made much smaller if some of the auxiliary components are removed and/or optimized.

Hall sensors are simply connected with the BLDC driver through input and output ports provided on the board, thus enabling modification of Hall sensor signals according to the proposed filtering and averaging methodologies. The proposed filter equations (4-8) and (4-16) in conjunction with averaging equations (4-20) - (4-22) were programmed on the microcontroller according to the implementation approach summarized in previous section and the functional diagrams depicted in Figure 4.5 and Figure 4.6.

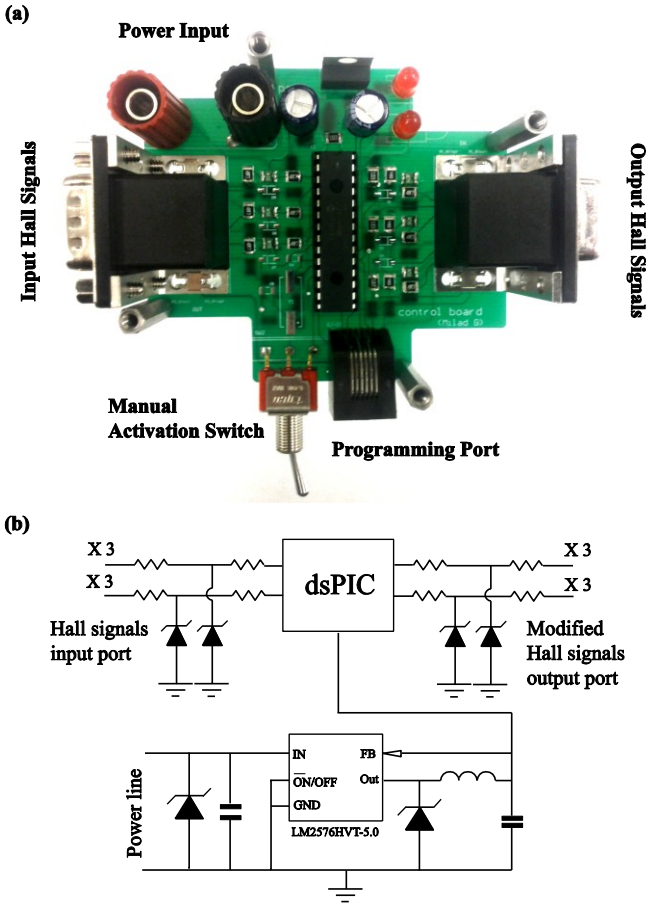

Figure 5.5 Prototype dongle-filter for use with existing motor drivers: (a) actual-size photo of the printed circuit board; and (b) simplified block-scheme representation depicting major components and ports.

5.3 Experimental Case Studies

To demonstrate operation of the proposed SLC dongle, a pair of BLDC motor-drives with the parameters summarized in Appendix B has been considered. In following studies, the motors are supplied with $V_{dc} = 30V$ and initially operate in an open loop control. To emulate driving different conditions, each motor is loaded by a dc machine dynamometer.

5.3.1 Sync-Lock Controller enabling Transient

To illustrate transient behavior of the proposed controller, motors are initially assumed to operate in steady state with 0.45 Nm on Motor 1 and 0.60 Nm on Motor 2, running at 1830 rpm and 1800 rpm, respectively. Then, the SLC is enabled. Following this change, both motors undergo a transient in measured currents and speed as depicted in Figure 5.6. This transient is due to the initial angle difference of the motors' shafts, which causes one of the motors to accelerate and the other motor to decelerate to

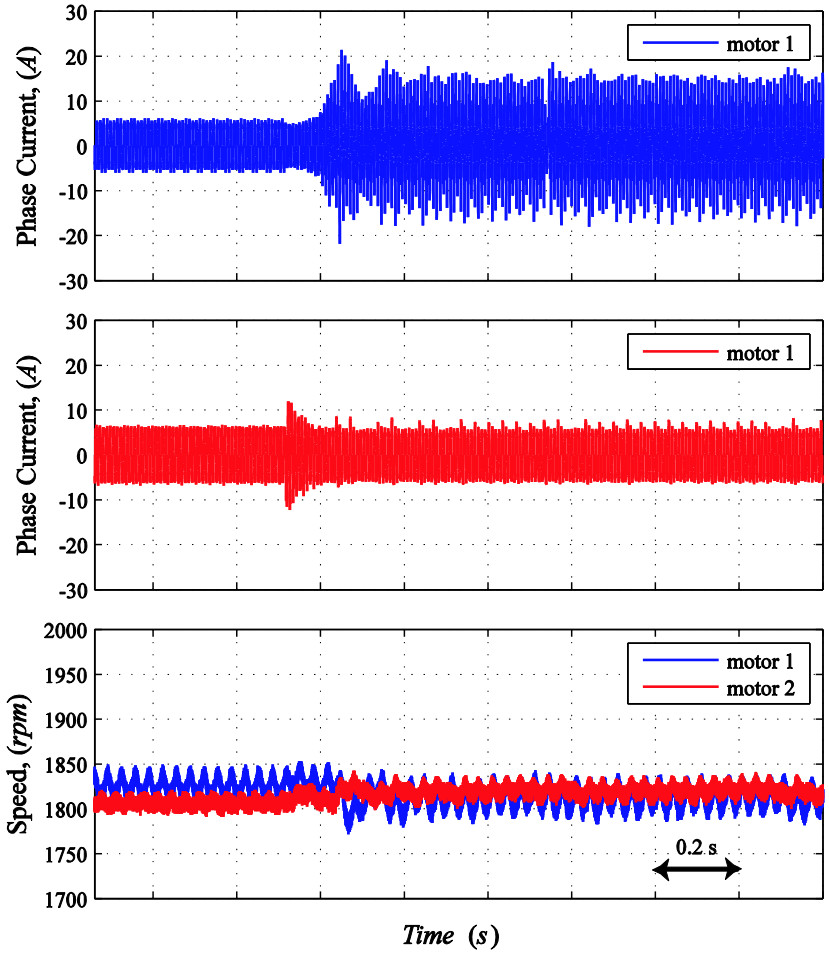

Figure 5.6 Measured phase current and speed transient response of both motors due to enabling the proposed SLC.

achieve locking. As can be seen in Figure 5.6, after the locking, currents are automatically adjusted to run both motors at same identical speed while satisfying their respective loads that are different.

5.3.2 Transient due to Change in Load

Performance of the locking mechanism is evaluated further by subjecting the system to a load disturbance. In the following study, both motors are assumed running at 1825 rpm while each driving a load of about 0.5 Nm. Then, the load on Motor 2 is increased as shown in Figure 5.7 and Figure 5.8 (first subplot). Resulting response of the motors' speed with the SLC disabled and enabled have been recorded and are approximately aligned in time and are also shown in Figure 5.7 and Figure 5.8 (second subplot), respectively. As it can be seen in Figure 5.7, when the SLC is disabled, increase in load on one of the motors does not couple to response of the other motor. However, when the SLC is enabled, motors remain locked and their speed in affected by changes in load of any one of the motors.

Continuing from previous experiment, the load on Motor 2 is stepped down while motors are locked. As shown in Figure 5.9, both motors remain synchronized and speed up to accommodate corresponding loads. System speed is determined by the average of speeds of two motors with slower motor carrying higher load as the reference (which is Motor 1 in this case). However, with proposed controller, there is no one master or slave motor always dictating system response or speed.

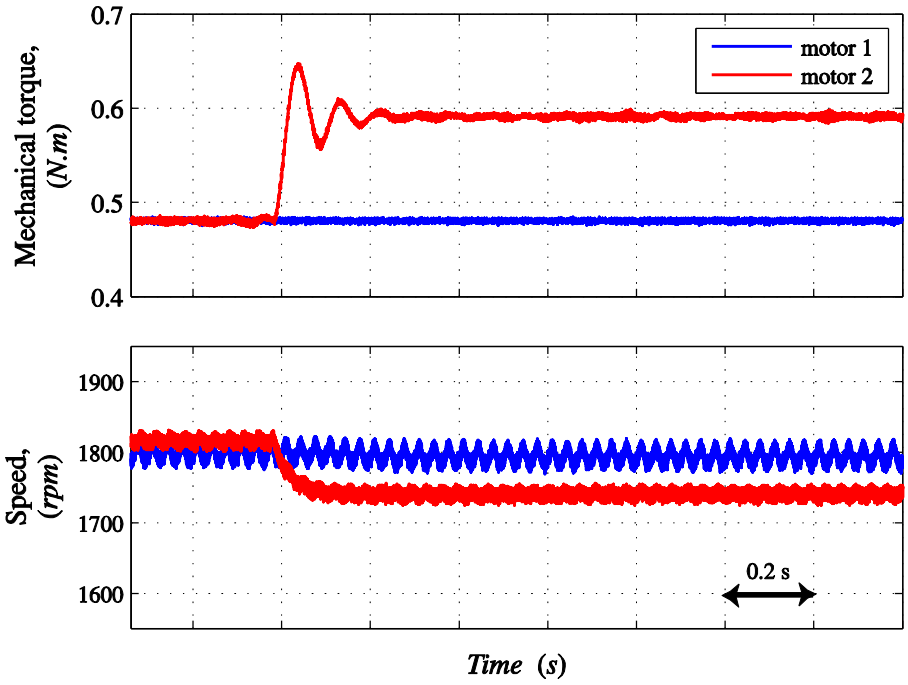

Figure 5.7 Measured mechanical torque and speed transient response due to load change with proposed SLC disabled.

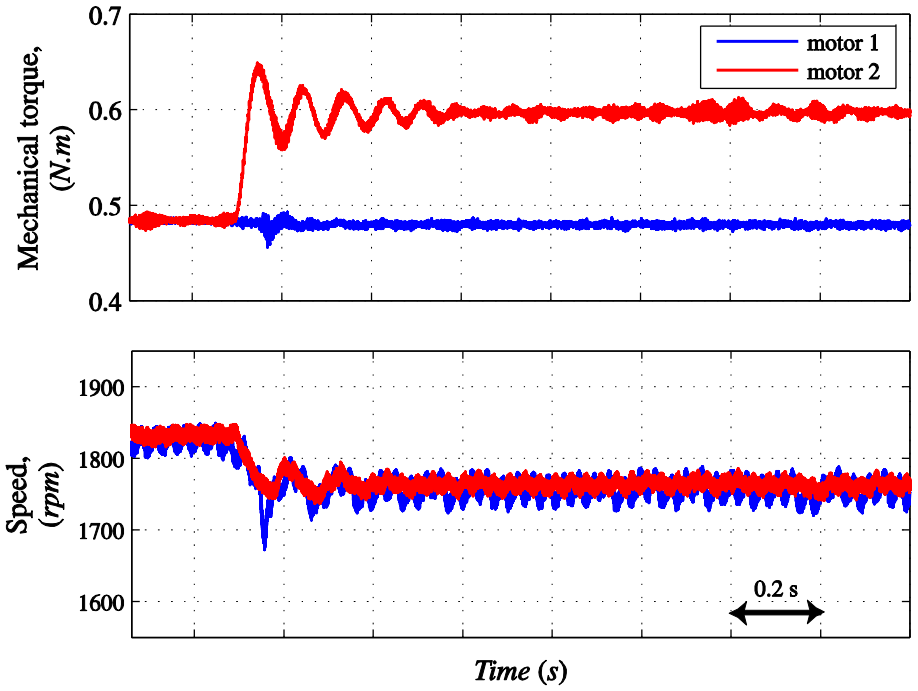

Figure 5.8 Measured mechanical torque and speed transient response due to load step up with proposed SLC enabled.

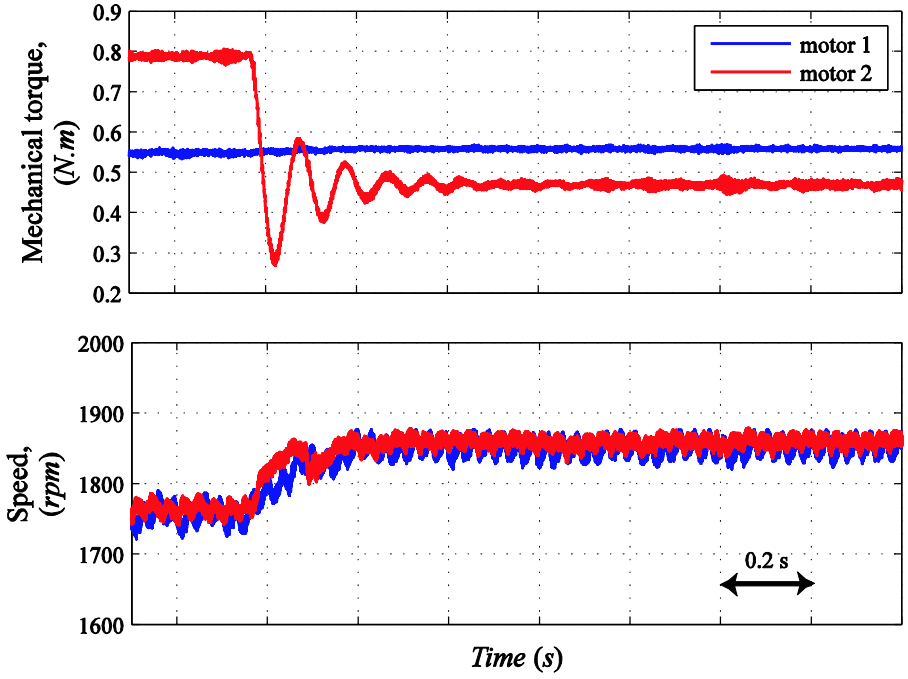

Figure 5.9 Measured mechanical torque and speed transient response due to load step down with proposed SLC enabled.

6 CONCLUSIONS AND FUTURE WORK

Today, electric vehicles are being considered as viable alternatives to the traditional internal combustion automobiles. A modern EV configuration with independent brushless DC (BLDC) machine-based wheel drives has been considered in this thesis. With the proposed independent wheel configuration, the mechanical differential is replaced with two traction BLDC motors that have no direct mechanical coupling, i.e. there is no common mechanical shaft connecting the two wheels together. Electric differential system is used to synchronize/lock the two motors together. Focus of this thesis is on locking the EDS of electric vehicles with independent BLDC machine-based wheel drives. The objective is to lock the active wheels of the vehicle as if they were operating on a common shaft.

6.1 Conclusion

In order to analyze the operation of independent wheel driven EV and study its control, a detailed computer model of the electric vehicle propulsion system has been developed and verified. The independent wheels are considered to be driven by Hall sensor controlled BLDC motors. The model includes the brushless dc (BLDC) motors that are voltage-source-inverter (VSI) driven and controlled by the conventional Hall sensors. Furthermore, the mechanical dynamics of the vehicle body and wheels are integrated to the electrical model of the drive system to complete the electric vehicle propulsion system model.

An innovative approach for synchronizing the vehicular driving wheels, thus emulating the locking electrical differential system (EDS) is proposed and integrated into the computer model of the vehicle propulsion system. The new Sync-Lock Controller is based on averaging the Hall sensor signals and applying the same switching intervals to both propulsion motors. An analog and a digital implementation of the proposed controller are developed and described in detail. As low-cost BLDC motors commonly have inaccurate Hall sensors, the hardware implementation also integrated filtering of the Hall sensor signals. Therefore desired locking is achieved by filtering and averaging the Hall sensor signals and applying the averaged switching intervals to both propulsion motors.

The digital implementation of the controller is realized using the microcontroller (dsPIC30f2020). The controller is realized in the form of a standalone dongle-circuit that can be placed between the original Hall-sensors and the motor drive to process the signals. A compact prototype of the proposed dongle had been fabricated and texted on a number of typical industrial BLDC motors and drivers. Due to its simplicity and effective implementation, the proposed algorithm can be readily applied to a variety of EVs that use BLDC motors and drivers. The performance of the proposed locking algorithm has been

demonstrated using BLDC motors (with Hall-sensor positioning errors) and is shown to be efficient and robust in steady state and transients studies. The performance of proposed SLC was evaluated under different conditions. It was shown that the SLC improves the performance of the vehicle under certain road conditions compared to the conventional PI speed control loops.

6.2 Future Work

This thesis was focused on locking the EDS with independent wheels in electric vehicle applications. Although the proposed controller is developed with EVs in mind, it should be mentioned that the controller could be utilized in any other mechanical and/or industrial application with multiple independently operated BLDC motors that are required to be locked/synchronized to achieve certain operational requirements. Hall sensor filter integrated into the proposed controller can also be further optimized by taking into account the uneven magnetization of the magnetic tablet as in [24].

Another extension of this project is consideration of equipment failure (specifically the Hall sensors), and further development of fail-safe strategies. With the proposed controller configured to modify Hall signals, it appears possible to add another layer of filtering to the system that could keep the operation of the motors stable even when one or more Hall sensors fail. For this extension, the proposed digital filtering approach will need to provide the drive system with a set of modified Hall signals based on the other two or even one operating Hall sensor.

BIBLIOGRAPHY

[1] E. H. Wakefield, History of the Electric Automobile: Battery-only Powered Cars, Society of Automotive Engineers (SAE), ISBN: 1-56091-299-5, Warrendale, PA, 1994.

[2] M.Ehsani, Y.Gao, S.E.Gay, and A.Emadi. Modern Electric Hybrid Electric, and Fuel Cell Vehicles: Fundamentals, Theory, and Design. CRC Press, Boca Raton, FL, 2005.

[3] P. C. Krause, O. Wasynczuk, S. D. Sudhoff, Analysis of Electric Machinery and Drive Systems. IEEE Press, Piscataway, NJ, 2002.

[4] J. P. Johnson, M. Ehsani, Y. Guzelgunler, "Review of Sensorless Methods for Brushless DC," In Proc. Industry Applications Conference, 1999. Thirty-Fourth IAS Annual Meeting. Conference Record of the 1999 IEEE, Vol. 1, pp. 143–150, Oct. 3 – 7, 1999.

[5] T. Senjyu, K. Uezato, "Adjustable Speed Control of Brushless DC Motors without Position and Speed Sensors," In Proc. Int'l. IEEE/IAS Conf. on Industrial Automation and Control: Emerging Technologies, pp. 160–164, 1995.

[6] A. Consoli, S. Musumeci, A. Raciti, A. Testa, "Sensorless Vector and Speed Control of Brushless Motor Drives," IEEE Trans. on Industrial Electronics, Vol. 41, pp. 91–96, February, 1994.

[7] P. Acarnley, "Sensorless Position Detection in Permanent Magnet Drives", IEE Colloquium on Permanent Magnet Machines and Drives, pp. 1011–1014, 1993.

[8] K. Iizuka, et al., "Microcomputer Control for Sensorless Brushless Motor," IEEE Transactions on Industry Applications, Vol. IA-27, pp. 595–601, May – June, 1985.

[9] W. Brown, "Brushless DC Motor Control Made Easy", Microchip Technology Inc., 2002. [Online]. Available: www.microchip.com

[10] K. R. Shouse, D. G. Taylor, "Sensorless Velocity Control of Permanent-Magnet Synchronous Motors", In Proc. 33rd Conf. on Decision and Control, pp. 1844–1849, December, 1994.

[11] N. Ertugrul, P. Acarnley, "A New Algorithm for Sensorless Operation of Permanent Magnet Motors," IEEE Transactions on Industry Applications, Vol. 30, pp. 126–133, January – February, 1994.

[12] N. Matsui, "Sensorless PM Brushless DC Motor Drives," IEEE Transactions on Industrial Electronics, Vol. 43, pp. 300–308, April, 1996.

[13] M Schrodl, "Sensorless Control of Permanent Magnet Synchronous Motors," Electric Machines and Power Systems, Vol. 22, pp. 173 – 185, 1994.

[14] B. J. Brunsbach, G. Henneberger, T. Klepseh, "Position Controlled Permanent Magnet Excited Synchronous Motor without Mechanical Sensors," In Proc. IEE Conf on Power Electronics and Applications, Vol. 6, pp. 38–43, 1993.

[15] M. Benarous, J.F. Eastham, P.C. Coles, "Sinusoidal Shaft Position Encoder," In Proc. Power Electronics, Machines and Drives (PEMD 2004), Vol. 1, Mar. 31 – Apr. 2, 2004 pp. 132–136

[16] Y. Buchnik, R. Rabinovici, “Speed and Position Estimation of Brushless DC Motor in Very Low Speeds,” In Proc. Convention of Electrical and Electronics Engineers in Israel, Sept. 6 – 7, 2004 pp. 317–320

[17] M. Gougani, M. Chapariha, J. Jatskevich, "Locking electric differential for brushless DC machine-based electric vehicle with independent wheel drives," Vehicle Power and Propulsion Conference (VPPC), 2011 IEEE , pp.1-6, 6-9 Sept. 2011.

[18] M. Gougani, M. Chapariha, J. Jatskevich, A. Davoudi, "Hall Sensor-Based Locking Electric Differential System for BLDC Motor Driven Electric Vehicles," International Electric Vehicle Conference (IEVC), 2012 IEEE , pp.1-7, 4-8 Mar. 2012.

[19] N. Samoylenko, Q. Han, J. Jatskevich, “Balancing hall-effect signals in low-precision brushless DC motors,” In Proc. IEEE Applied Power Electronics Conference, Feb. 28 – Mar. 2, 2007, Anaheim CA, USA, pp. 606–611.

[20] N. Samoylenko, Q. Han, J. Jatskevich, “Improving dynamic performance of low-precision brushless DC motors with unbalanced Hall sensors,” In Proc. IEEE Power Engineering Society General Meeting, Panel Session – Intelligent Motor Control I, June 24–28, 2007, Tampa FL, USA.

[21] P. Alaeinovin, “Analysis and improvement of low precision Hall-sensor-controlled brushless dc motors,” M.S. thesis, Dept. Elect. Eng., Univ. British Columbia, Vancouver, 2010.

[22] Simulink: Dynamic System Simulation for MATLAB, Using Simulink Version 7.3, The MathWorks Inc., 2009a.

[23] Automated State Model Generator (ASMG), Reference Manual Version 2, P.C. Krause & Associates, Inc. 2003.

[24] N. Samoylenko, H. Qiang, J. Jatskevich, "Dynamic Performance of Brushless DC Motors with Unbalanced Hall Sensors," Energy Conversion, IEEE Transactions on, vol.23, no.3, pp.752-763, Sept. 2008.

[25] P. Pillay, R. Krishnan, “Modeling, simulation, and analysis of permanent-magnet motor drives. Part II. The brushless DC motor drive,” IEEE Transactions on Industry Applications, Vol. 25, Iss. 2, March-April 1989, pp. 274-279.

[26] S. D. Sudhoff, P. C. Krause, “Average-value Model of the Brushless DC 120º Inverter System,” IEEE Transactions on Energy Conversion, Vol. 5, No. 3, pp. 553-557, 1990.

[27] S. D. Sudhoff, P. C. Krause, “Operation Modes of the Brushless DC Motor with a 120º Inverter,” IEEE Transactions on Energy Conversion, Vol. 5, No. 3, pp. 558-564, 1990.

[28] P. L. Chapman, S. D. Sudhoff, C. A. Whitcomb, “Multiple Reference Frame Analysis of Non-sinusoidal Brushless DC Drives,” IEEE Transactions on Energy Conversion, Vol. 14, No. 3, pp. 440-446, 1999.

[29] W-S.Kim, Y-S.Kim, J-K.Kang, and S-K.Sul, "Electro-mechanical re-adhesion control simulator for inverter-driven railway electric vechicle", Conference Record of the 1999 IEEE Industry Applications Conference, 2:1026-1032, 1999.

[30] Y. Takaoka, A. Kawamura, "Disturbance Observer Based Adhesion Control for Sinkansen", AMC2000-NAGOYA, 2000, pp.169-174.

[31] F. Rodriguez, A. Emadi, “A Novel Digital Control Technique for Brushless DC Motor Drives” IEEE Trans. Industrial Electronics Vol. 54, Iss. 5, pp. 2365–2373, Oct. 2007.

[32] Pan Ching-Tsai, E. Fang, “A Phase-Locked-Loop-Assisted Internal Model Adjustable-Speed Controller for BLDC Motors” IEEE Trans. Industrial Electronics Vol. 55, Iss. 9, pp. 3415–3425, Sep. 2008.

[33] S. Rajagopalan, J. M. Aller, J. A. Restrepo, T. G. Habetler, R.G .Harley, “Analytic-Wavelet-Ridge-Based Detection of Dynamic Eccentricity in Brushless Direct Current (BLDC) Motors Functioning Under Dynamic Operating Conditions” IEEE Trans. Industrial Electronics Vol. 54, Iss. 3, pp. 1410–1419, Jun. 2007.

[34] Chung-Wen Hung, Cheng-Tsung Lin, Chih-Wen Liu, “Fuzzy PI Controller for BLDC motors Considering Variable Sampling Effect” In Proc. 33rd Annual Conf. of the IEEE Industrial Electronics Society (IECON), Nov. 5-8, 2007, Taipei, Taiwan, pp. 1175–1179.

[35] A. Sathyan, N. Milivojevic, Y. J. Lee, M. Krishnamurthy, A. Emadi, “An FPGA Based Novel Digital PWM Control Scheme for BLDC Motor Drives,” Accepted to IEEE Trans. Industrial Electronics, (Paper TIE.2009.2022067).

[36] Dan Liu, Changliang Xia, Maohua Zhang, Yingfa Wang, “Control of Brushless DC Motor Using Fuzzy Set Based Immune Feedback PID Controller,” In Proc. IEEE International Symposium on Industrial Electronics (ISIE 2007), 4-7 June 2007, pp. 1045–1049.

[37] P. B. Beccue, S. D. Pekarek, B. J. Deken, A. C. Koenig, “Compensation for asymmetries and misalignment in a Hall-effect position observer used in PMSM torque-ripple control,” IEEE Trans. Industry Applications, Vol. 43, No. 2, pp. 560–570, 2007.

[38] B. Tabbache, A. Kheloui, N. Hanini, "An electric differential system for a two-wheel mobile plat-form using direct torque control with adaptive flux and speed observers," Power Electronics, Electrical Drives, Automation and Motion, 2008. SPEEDAM 2008. International Symposium on , vol., no., pp.550-556, 11-13 June 2008

[39] J. G. Proakis, D. G. Manolakis, Digital Signal Processing, Prentice Hall, Upper Saddle River, NJ, 1996, p. 248.

[40] dsPIC30f1010/202x Data Sheet, 28/40/44-Pin High-Performance Switch Mode Power Supply Digital Signal Controllers. Microchip Technology Inc., 2006 [Online]. Available: www.microchip.com

[41] Reston Condit “Sensorless BLDC with Back-EMF Filtering,” Microchip Technology Inc. Available: http://ww1.microchip.com/downloads/en/AppNotes/01083a.pdf

[42] J.Larminie and J.Lowry. Electric Vehicle Technology Explained. John Wiley & Sons, West Sussex, England, 2003.

[43] D. Juan, M. Ortuzar, Tests results with regenerative braking based on super-capacitors and a buck-boost converter. Berlin, 2001

APPENDICES

Appendix A: Parameters used for Studies in Chapters 2 and 3

BLDC PROPULSION MOTOR PARAMETERS:

eCycle Inc., Model MGA-1-13, 4.5 kW, 12 poles, $r_s = 0.027\Omega$, $L_s = 0.025mH$, $\lambda_m^{'} = 10.9mV.s$, rotor inertia $J_{rot} = 0.005kg.m^2$, back EMF harmonics coefficients $K_3 = -0.206$, $K_5 = 0.047$, $K_7 = -0.0067$.

MECHANICAL PARAMETERS:

Mass of the vehicle, $M_v = 190kg$, mass of the wheel, $M_w = 10kg$, load inertia, $J_{load} = 0.02kg.m^2$, damping coefficient, $B_m = 0.05N.s$, radius of the wheel, $r = 0.05m$, gravitational constant, $g = 9.81m/s^2$, and controller coefficients $K_p = 0.012$, $K_i = 0.0161$.

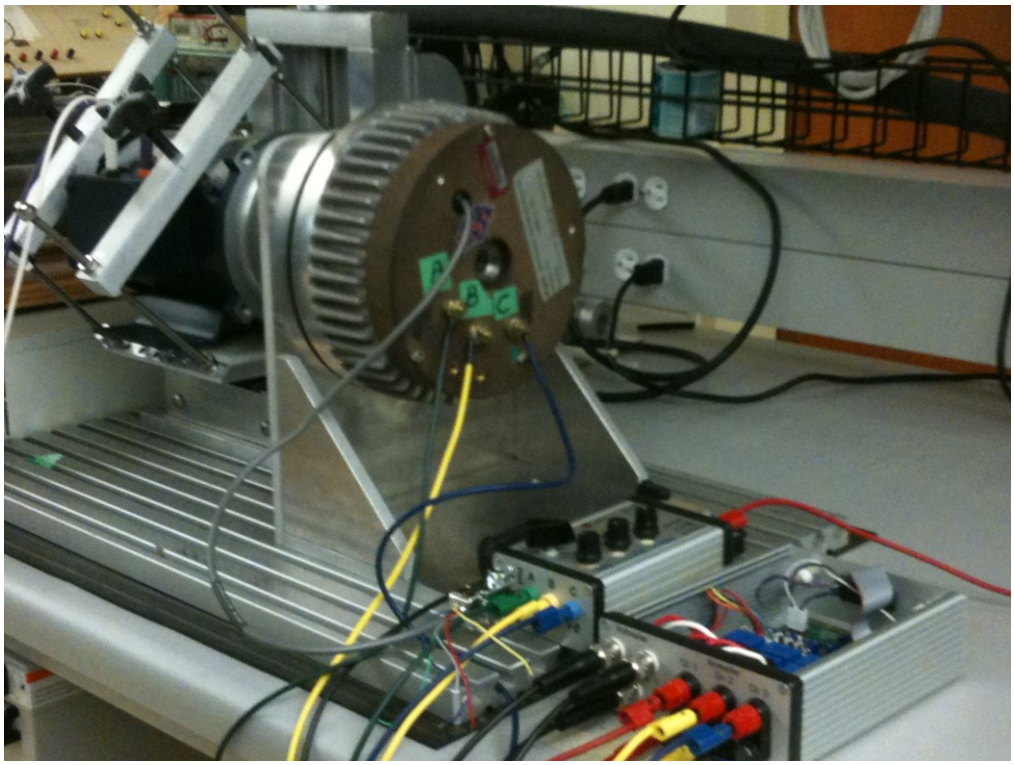

Appendix B: Parameters used for Studies in Chapter 4 and 5

BLDC PROPULSION MOTOR PARAMETERS:

Arrow Precision Motor Co., LTD., Model 86EMB3S98F, 36 VDC, 210 W, 2000 rpm, 8 poles, $r_s = 0.12\Omega$, $L_s = 0.375mH$, $\lambda_m^{'} = 22mV.s$, combined inertia $J = 12 \cdot 10^{-4} N.m.s^2$, and back EMF harmonics coefficients $K_3 = 0.01$, $K_5 = -0.059$, $K_7 = 0.025$.

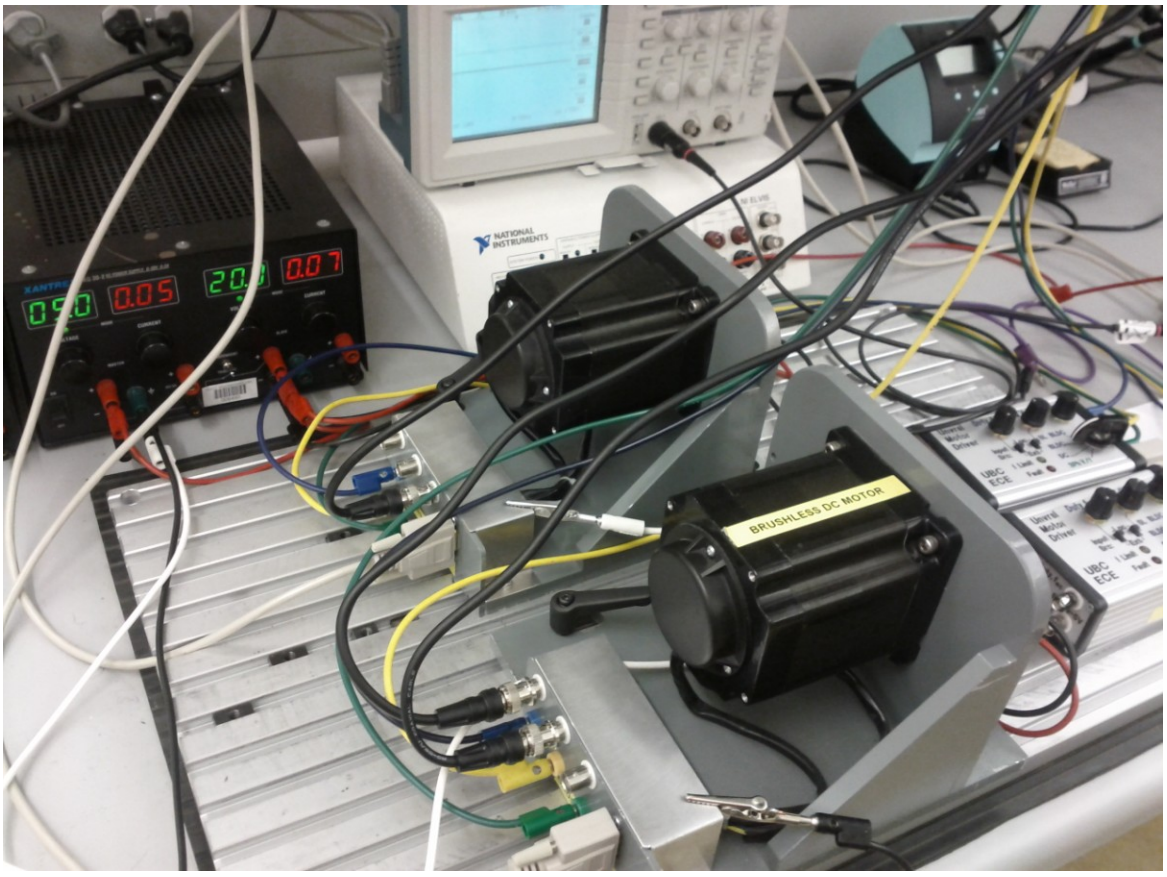

Appendix C: Designed PCB Schematic

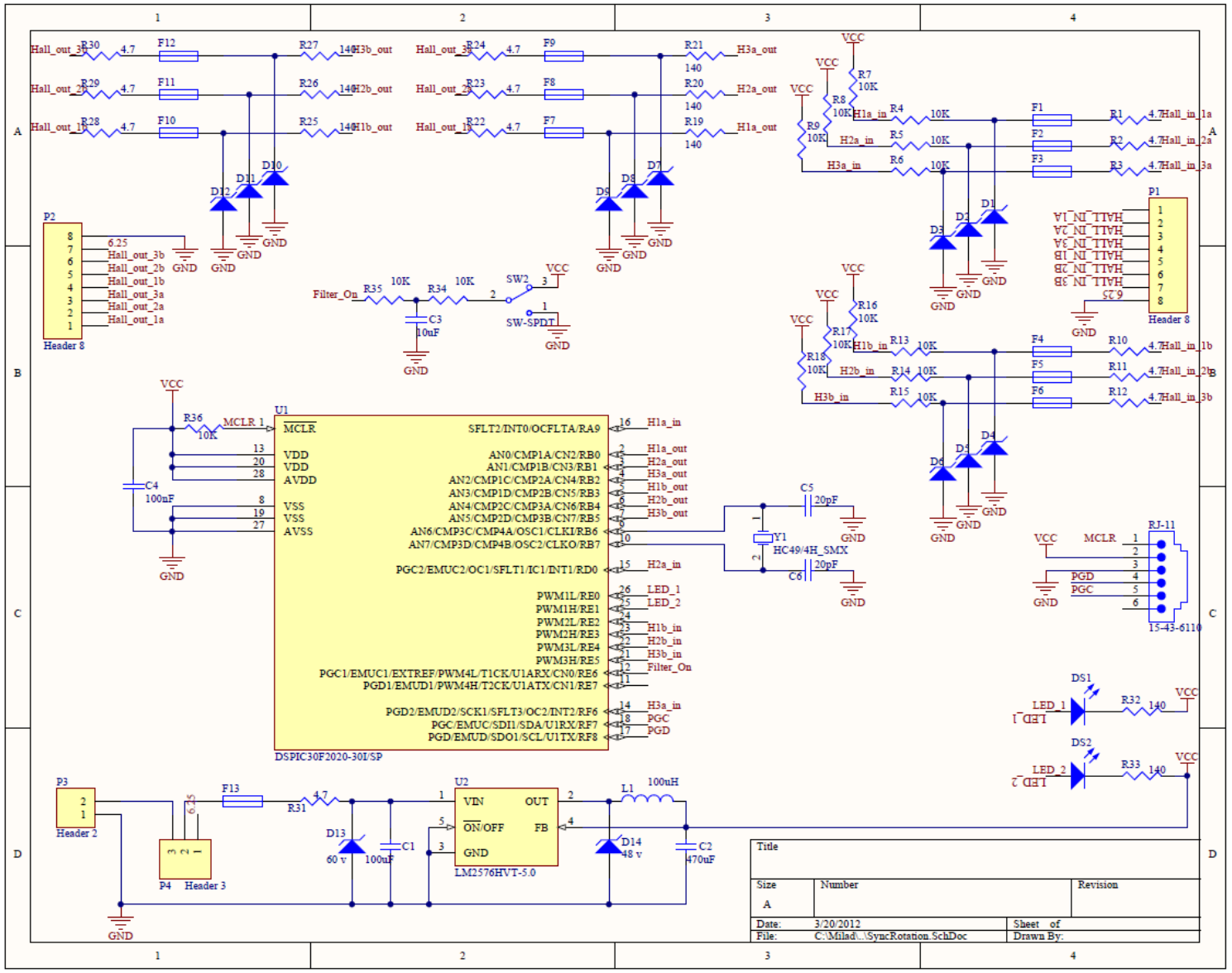

Appendix D: Designed PCB Layout (Double Sided)